Check for updates

AGU100 ADVANCING EARTH AND SPACE SCIENCE

JGR

Journal of Geophysical Research: Solid Earth

RESEARCH ARTICLE

10.1029/2017JB015066

Key Points:
- Late Cenozoic volcanism in southwest Japan arc is characterized by bimodal eruptions of andesite and dacite lavas and basalt lavas with SiO_2 gap from 55 to 58 wt %
- Andesite and dacite lavas are enriched in Sr (mostly >800 μg g^{-1}) and show geochemical compositions consistent with the magmas derived from melting of subducted oceanic crust
- Spatial coincidence of the occurrence of high-Sr andesite and dacite volcanoes and seismic gaps of the subducting lithosphere suggests that slab melting is likely to occur at tears on the slab with thermal ablation by mantle flow

Supporting Information:
- Supporting Information S1

Correspondence to:
I. Pineda-Velasco,
ivan_pineda@okayama-u.ac.jp

Citation:
Pineda-Velasco, I., Kitagawa, H., Nguyen, T. -T., Kobayashi, K., & Nakamura, E. (2018). Production of high-Sr andesite and dacite magmas by melting of subducting oceanic lithosphere at propagating slab tears. *Journal of Geophysical Research: Solid Earth*, *123*, 3698–3728. https://doi.org/10.1029/2017JB015066

Received 2 OCT 2017
Accepted 29 APR 2018
Accepted article online 5 MAY 2018
Published online 30 MAY 2018

Production of High-Sr Andesite and Dacite Magmas by Melting of Subducting Oceanic Lithosphere at Propagating Slab Tears

I. Pineda-Velasco[1], H. Kitagawa[1], T. -T. Nguyen[1], K. Kobayashi[1], and E. Nakamura[1]

[1]Pheasant Memorial Laboratory, Institute for Planetary Materials, Okayama University at Misasa, Tottori, Japan

Abstract We present K-Ar ages, major and trace element concentrations, and Sr-Nd-Pb isotope data for late Cenozoic volcanic rocks from the Chugoku district, southwest Japan arc. Andesite and dacite lavas in this region are enriched in Sr (mostly >800 μg g^{-1}) and show geochemical characteristics of volcanic rocks commonly referred to as "adakite." K-Ar dating of these lavas revealed that the eruption of high-Sr andesitic to dacitic magmas occurred during the last 2 Myr, following or concurrent with the eruption of basalt in adjacent regions. Trace-element characteristics of high-Sr andesites and dacites are consistent with the formation of their parent magmas by partial melting of the basaltic layer of the subducting Shikoku Basin Plate. Mass balance modeling of trace element concentrations and isotopic compositions suggests that the parental magmas of high-Sr andesites and dacites are best explained by mixing of partial melts from oceanic crust (F = 5–15%) and sediment (F = 30%) at 80:20 to 55:45 ratios. Spatial coincidence of the occurrences of high-Sr andesites and dacites and seismic gaps of the subducting slab demonstrates the causal link between slab melting and mantle upwelling at slab tears. We speculate that these tears could have been formed by subduction of ridges on the plate. A warm mantle upwelled through tears, preventing the solidification of the siliceous slab melts in the mantle and facilitating the transportation of these melts to the surface.

1. Introduction

In subduction zone, oceanic lithosphere sinks into the mantle and the crustal layer of subducting oceanic lithosphere (slab) progressively metamorphoses with increasing depth. Fluids released from the slab lead to hydration and melting of the overlying mantle and formation of volcanic arcs (Ishikawa & Nakamura, 1994; Nakamura et al., 1985; Sakuyama & Nesbitt, 1986).

When a young (<25 Myr) and hot slab subducts, it can partially melt leading to the evolution of magmas of intermediate to felsic compositions. Defant and Drummond (1990) noted peculiar geochemical characteristics of these magmas such as high-Sr abundance and referred to such magma as adakite, in reference to its first documented occurrence on the island of Adak in the Aleutians (Kay, 1978). Because adakite is a silica-saturated melt, it is expected to react with peridotite during percolation in the mantle (Kelemen et al., 1998). Such reaction is expected to consume melts and form pyroxenite, and the melts could have little chance of reaching the surface. However, reaction during adiabatic decompression could allow the slab melts to survive in the mantle (Kelemen et al., 1993), and several studies of natural samples have presented evidence to support this idea (e.g., the occurrence of Sr-rich felsic-melt veins in peridotite xenoliths; Kepezhinskas et al., 1996).

Melt-mantle interaction accompanies mass transfer reaction which modifies the element concentrations in the melt and mantle (Kelemen et al., 1993, 1998). Slab-derived melts generally have greater element solubilities than aqueous fluids (Kessel, Schmidt, et al., 2005; Klimm et al., 2008); thus, melt metasomatism produces peculiar geochemical signatures, such as enrichments of fluid-immobile incompatible elements, in the subarc mantle (Defant & Kepezhinskas, 2001). Previous studies documented the occurrence of various basaltic magmas associated with adakitic high-Sr andesites and dacites, including ocean-island-type alkaline basalt and island arc-type subalkaline basalt and andesite (Kimura et al., 2014; Leeman et al., 1990). Genesis of these magmas could be attributed to melting of mantle interacted with varying extents of slab-derived melt.

The southwest (SW) Japan arc (Figure 1) is an example of a volcanic field in which high-Sr andesites and dacites occur (Figure 2; Feineman et al., 2013; Kimura et al., 2014; Morris, 1995). Like others, the SW Japan arc is characterized by the occurrence of basalt lavas in closed spatial and temporal proximity. It is

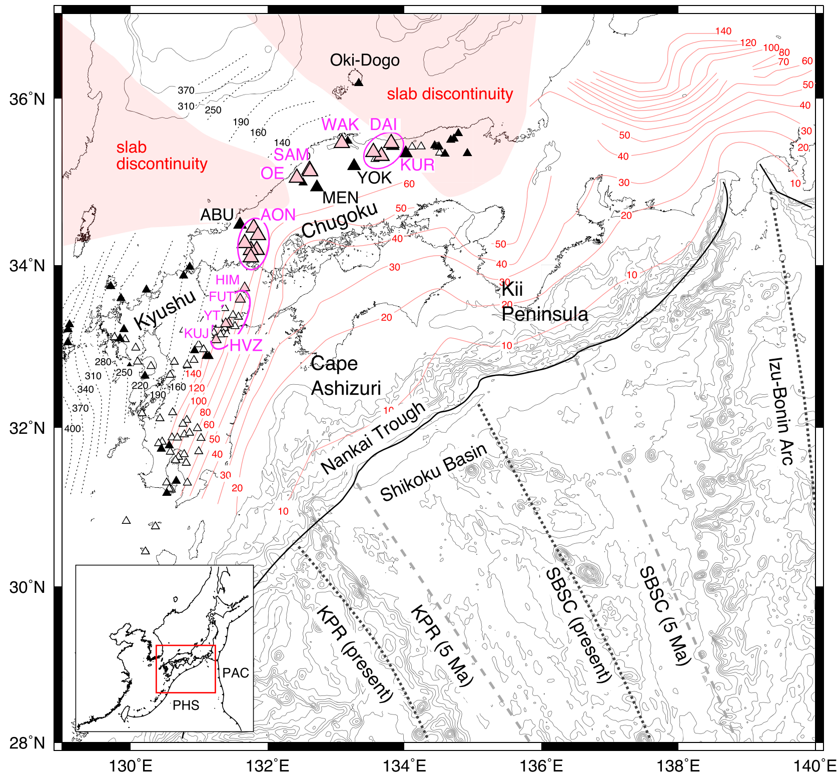

Figure 1. A map of the southwest Japan arc, showing distribution of Quaternary volcanoes, geological and topographic features of Shikoku Basin, and seismic property of the subducting plate. Locations of Quaternary volcanoes are shown with triangle (black, basalt; open, island arc type andesite-dacite-rhyolite; pink, high-Sr andesite and dacite; Nishiki et al., 2012): KUR, Kurayoshi; DAI, Daisen; WAK, Wakurayama; YOK, Yokota; SAM, Sambe; OE, Oe-Takayama; MEN, Mengame; AON, Aonoyama; ABU, Abu; HIM, Himeshima; HVZ, Hohi volcanic zone; FUT, Futagoyama; YT, Yufu-Tsurumi; KUJ, Kuju. Present and past (5 Ma) positions of Shikoku Basin spreading center (SBSC) and Kyushu-Palau Ridge (KPR) are shown after Mahony et al. (2011). Depth (in km) of the top of subducting slab is shown with contour line (black dotted line, the aseismic slab; red line, seismic slab; Zhao et al., 2012). Discontinuity of slab is observed in the mantle beneath the north of Abu and Kurayoshi areas. Note that the slab discontinuities are located at the northwestern extensions of KPR and SBSC at 5 Ma. An inset shows the location of southwest Japan and plate configuration (PAC, Pacific Plate; PHS, Philippine Sea Plate). The basemap is created using Generic Mapping Tools (Wessel et al., 2013).

generally accepted that these andesites and dacites in SW Japan are attributed to melting of the subducted plate in late Cenozoic time (Feineman et al., 2013; Kimura et al., 2014; Morris, 1995; Shibata et al., 2014). Recent studies also argued the condition of slab melting and percolation through the mantle (Kimura, 2017; Kimura et al., 2014). However, the genesis of high-Sr andesites and dacites and associated basalts is still poorly constrained in conjunction with the structure of subducting oceanic lithosphere. In this study, we examined geochronological and geochemical properties of late Cenozoic high-Sr andesites and dacites and associated basalt lavas. These data are used to elaborate on the genetic relationship between the basalts and high-Sr andesites and dacites in order to constrain the nature and extent of slab-mantle interaction. We then discuss the use of these volcanic occurrences as tracers of slab morphology and, integrating our results with seismic tomography, we provide a model for the late Cenozoic evolution of the subducting plate beneath SW Japan.

2. Tectonic and Geologic Background

The young marginal Shikoku Basin, on the Philippine Sea Plate, is subducting beneath SW Japan, with two chains of topographic prominence currently subducting into the Nankai Trough: Kyushu-Palau Ridge (KPR) in the west and Shikoku Basin Spreading Center (SBSC) in the east (Figure 1). These ridges were formed by subduction of Pacific Plate beneath the Philippine Sea Plate; KPR is a remnant island arc formed during 48–25 Ma (Ishizuka et al., 2011), and SBSC is a remnant back-arc basin formed during 26–15 Ma (Okino et al., 1994).

Late Cenozoic volcanic rocks are distributed widely in SW Japan, including in the northern Kyushu and Chugoku districts (Figure 1). The volcanism in the Chugoku district has been active during the last 12 Myr

10.1029/2017JB015066

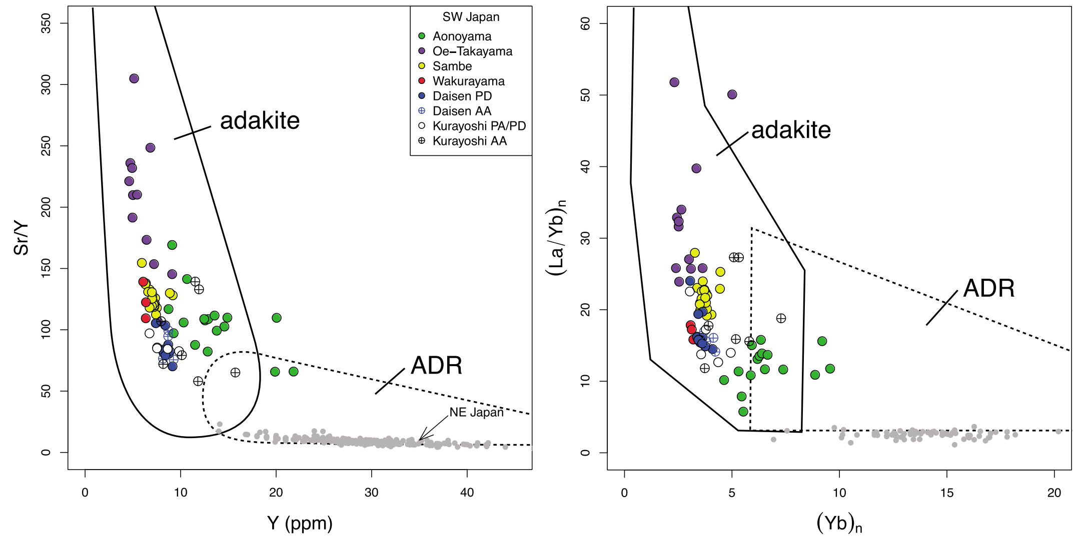

Figure 2. The Y-Sr/Y and $(Yb)_n$-$(La/Yb)_n$ diagrams showing adakitic signature of late Cenozoic andesite and dacite lavas from Aonoyama, Oe-Takayama, Sambe, Wakurayama, Daisen, and Kurayoshi in Chugoku district, SW Japan: AA, aphyric andesite; PA, porphyritic andesite; PD, porphyritic dacite. Data for Daisen PD and AA are from Feineman et al. (2013). Data for andesite-dacite-rhyolite suite (ADR) from Quaternary NE-Japan volcanoes are also shown for comparison (Ban & Yamamoto, 2002; Hunter & Blake, 1995; Kimura & Yoshida, 2006; Kimura et al., 2002; Kudo et al., 2007; Kuritani, Yoshida, Kimura, Hirahara, et al., 2014; Kuritani, Yoshida, Kimura, Takahashi, et al., 2014; Moriguti et al., 2004; Ohba et al., 2009; Sakuyama & Nesbitt, 1986; Takahashi et al., 2013; Tatsumi et al., 2008; Toya et al., 2005; Ueki & Iwamori, 2017; Tables S35 and S36). The compositional fields of adakite and nonadakitic ADR lavas are after Defant and Drummond (1990) and Martin (1999).

(Kimura et al., 2014, 2003, 2005; Uto, 1990) and shows systematic temporal variation in terms of mode of eruption and geochemistry of volcanic rocks. In the first 6 Myr (12–6 Ma), the magmatism is dominated by monogenetic eruptions of intraplate-type alkaline basalts. Volcanic ejecta form a cluster with diameter typically 20 km. Such a cluster is recognized as a discrete volcanic province, and it is distributed widely in this district (Kimura et al., 2003, 2005). Based on its geochemistry, the magmatism is attributed to melting of a hot and buoyant mantle with minimal subduction inputs (Iwamori, 1991; Nakamura et al., 1989).

Later magmatism (6–0 Ma) is characterized by eruptions of geochemically variable rocks. These rocks consist of subalkaline basalt and andesite including magnesian andesite (nonadakitic) and alkaline basalts with ultrasodic and ultrapotassic suites (Iwamori, 1991; Kimura et al., 2003; Koyaguchi, 1986; Nakamura et al., 1990; Shukuno & Arai, 1999; Tatsumi et al., 1999). In particular, the magmatism in the last 2 Myr is dominated by voluminous emplacement of high-Sr andesites and dacites (adakitic; Kimura et al., 2005; Figure 2).

Six volcanic fields are recognized as containing high-Sr andesites and dacites in Chugoku district (Feineman et al., 2013; Morris, 1995) and four fields in Kyushu (Shibata et al., 2014); Aonoyama, Oe-Takayama, Sambe, Wakurayama, Daisen, and Kurayoshi in Chugoku district and Himeshima, Futagoyama, Yufu-Tsurumi, and Kuju in Kyushu district. These andesite-dacite suites are located at the volcanic front above the depth contours of 80–100 km for the top of the subducting Shikoku Basin Plate (Figure 1). In the Chugoku district, the high-Sr andesite and dacite volcanic activities are associated with monogenetic basalt eruptions (Feineman et al., 2013; Kimura et al., 2014).

2.1. Aonoyama

The Aonoyama volcanic field is located in the western Chugoku district (Figures 1 and 3), and consists of 22 andesitic-dacitic lava domes unconformably overlying Permian metamorphic rocks and Cretaceous felsic rocks (Furuyama et al., 2002; Kumura et al., 2002). Based on their basal diameters ($<$2 km) and relative heights ($<$500 m), the volumes of the domes are estimated as being $<$1 km^3, leading to a total eruptive volume of about 20 km^3.

The basaltic volcanism, consisting of 50–60 centers, occurred in the Abu volcanic field, located in northwest part of the Aonoyama volcanic field (Kakubuchi et al., 2000; Koyaguchi, 1986; Uto & Koyaguchi, 1987). Various types of mafic volcanic rocks occur in this region, including alkaline basalt, subalkaline basalt, ultrapotassic basalt (shoshonite), and magnesian andesite (Kakubuchi et al., 2000; Kimura et al., 2014; Koyaguchi, 1986;

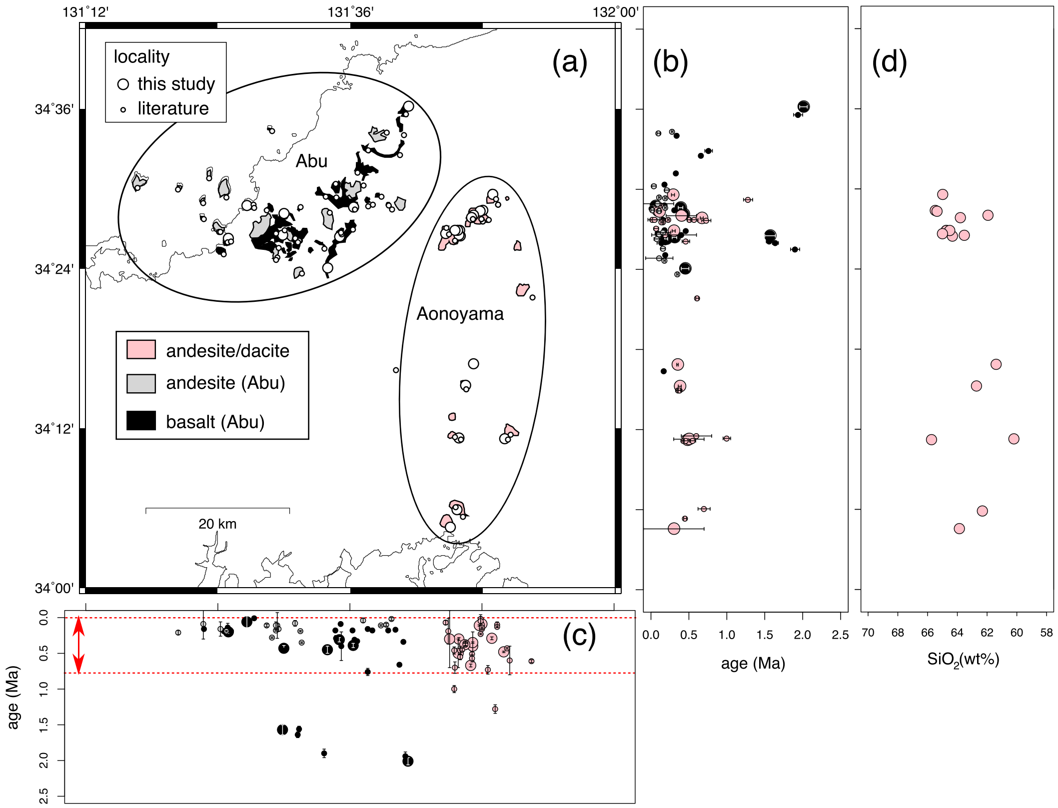

Figure 3. Distribution of high-Sr andesites and dacites and basalt lavas in Aonoyama and Abu volcanic fields. (a) Occurrence of high-Sr andesites and dacites and basalt lavas and the locality of studied lavas. (b) Latitudinal variation in K-Ar ages. (c) Longitudinal variation in K-Ar ages. The red arrow indicates the period of concurrent activity of basalt and high-Sr andesite and dacite adakitic magmas. The size of symbol denotes data source: large circle, this study (Tables S11 and S13); small circle, literature (Furuyama et al., 2002; Kakubuchi et al., 2000; Kamata et al., 1987; Kimura et al., 2003; Kumura et al., 2002; Uto & Koyaguchi, 1987; Tables S16 and S17). (d) Latitudinal variation in SiO_2 abundance of high-Sr andesite and dacite lavas. In (b)–(d), rock types are indicated by color: black, basalt; gray, andesite; pink, high-Sr andesite and dacite (andesite/dacite). Uncertainty on age is $1\sigma_m$.

Tatsumi & Koyaguchi, 1989). It is noted that magnesian andesites in this volcanic field have low Sr/Y (<50, i.e., nonadakitic; Kimura et al., 2014), and some of them exhibit petrographic features suggestive of magma mixing of alkaline basalt and dacite in crustal magma reservoirs (e.g., disequilibrium assemblage of phenocrysts; Koyaguchi, 1986).

2.2. Oe-Takayama and Sambe

The Oe-Takayama and Sambe are volcanic complexes located in the central Chugoku district (Figures 1 and 4) and located in 20 km from each other. The Oe-Takayama volcano consists of dacitic lava domes and pyroclastic deposits unconformably overlying the late Cretaceous felsic volcanic and plutonic rocks (Kano et al., 2000). The stratigraphy is poorly constrained due to substantial dissection of the volcano.

Sambe volcanic complex consists of pumice fall deposits and andesitic and dacitic lavas, all of which unconformably overlie the late Cretaceous granites (Matsui & Inoue, 1970). Four events of lava-flow emplacement have been documented based on volcanostratigraphy: Moritayama, Hikageyama, Kitanohara, and Sambe-dome lavas, respectively, from the lower to upper sequence (Hattori et al., 1983).

Basaltic lavas occur at Mengame volcano, located 20 km southeast of Sambe. That volcano consists of olivine-basalt flows and minor pyroclastic rocks unconformably overlying the Cretaceous rhyolite and Paleogene granite (Matsuura, 1986; Zellmer et al., 2014, 2015).

2.3. Wakurayama, Daisen, and Kurayoshi

Wakurayama, Daisen, and Kurayoshi volcanic fields are located in the eastern part of the Chugoku district (Figures 1 and 5). The Wakurayama volcano consists mainly of aphyric dacite lavas with subordinate

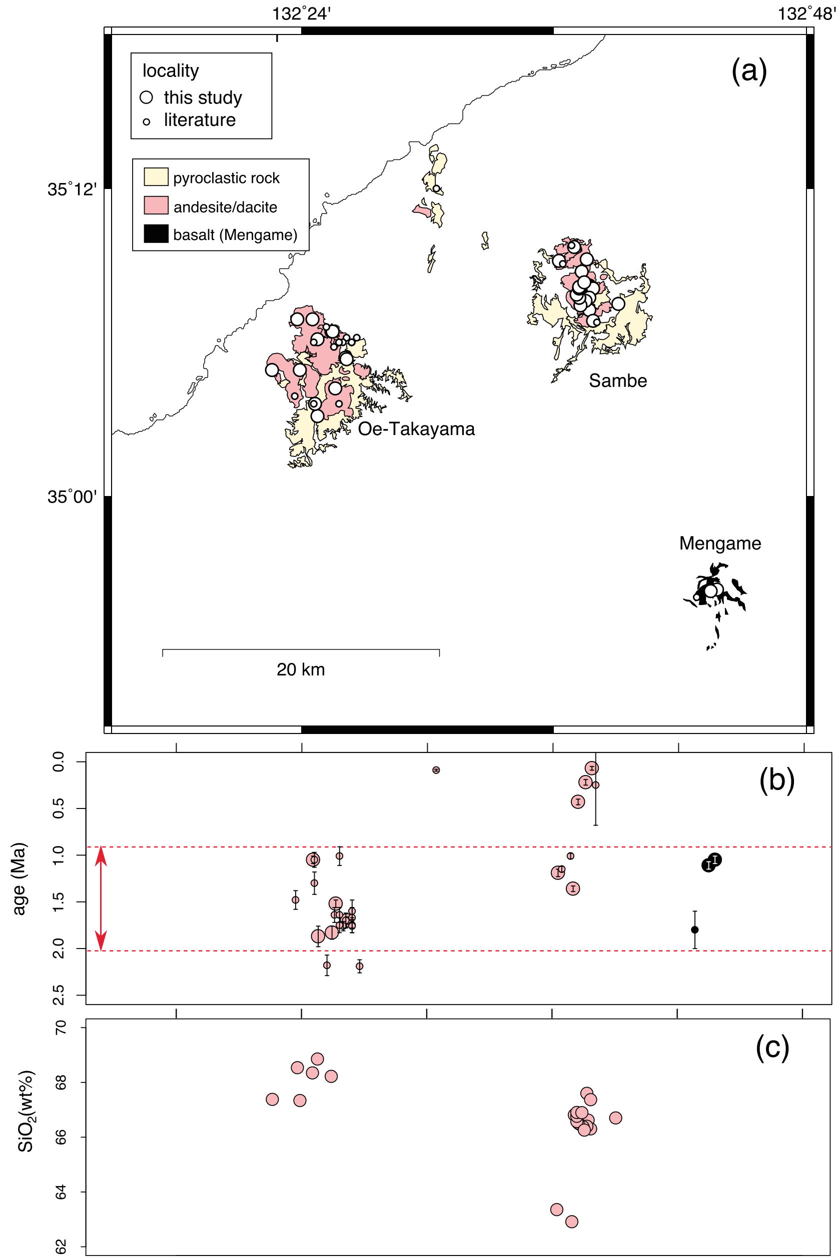

Figure 4. Distribution of high-Sr andesites and dacites and basalt lavas in Oe-Takayama, Sambe, and Mengame volcanic fields. (a) Occurrence of high-Sr andesites and dacites and basalt lavas and the locality of studied lavas. (b) Longitudinal variation in K-Ar age. The red arrow indicates the period of concurrent activity of high-Sr andesites and dacites and basalt magmas. Size of symbol denotes data source: large circle, this study (Tables S11 and S13); small circle, literature (Kano et al., 2000; Kimura et al., 2003; Matsuura, 1986; Matsuura & Tsuchiya, 2003; Miura & Sawai, 2010; Sakoda et al., 2000; Table S18). (c) Longitudinal variation in SiO_2 abundance of high-Sr andesite and dacite lavas. In (b) and (c), rock types are indicated by color: black, basalt; pink, high-Sr andesite and dacite. Uncertainty on age is $1\sigma_m$.

pyroclastic rocks. The lavas unconformably overlie the middle Miocene sediment and volcanic rocks (Sato et al., 2011).

Daisen volcano is the most voluminous eruption of andesite and dacite in SW Japan (Tsukui, 1984) and here lavas and pyroclastic fall deposits unconformably overlie basement rocks (Jurassic and Cretaceous granites and gneisses; Ishiga et al., 1989; Tsukui et al., 1985). Two types of lava are recognized based on modal mineral composition (Tsukui et al., 1985). The porphyritic dacitic lavas are volumetrically predominant and form lava domes, whereas the aphyric andesitic lavas are volumetrically minor and occur in the western flank of the complex (Figure 5).

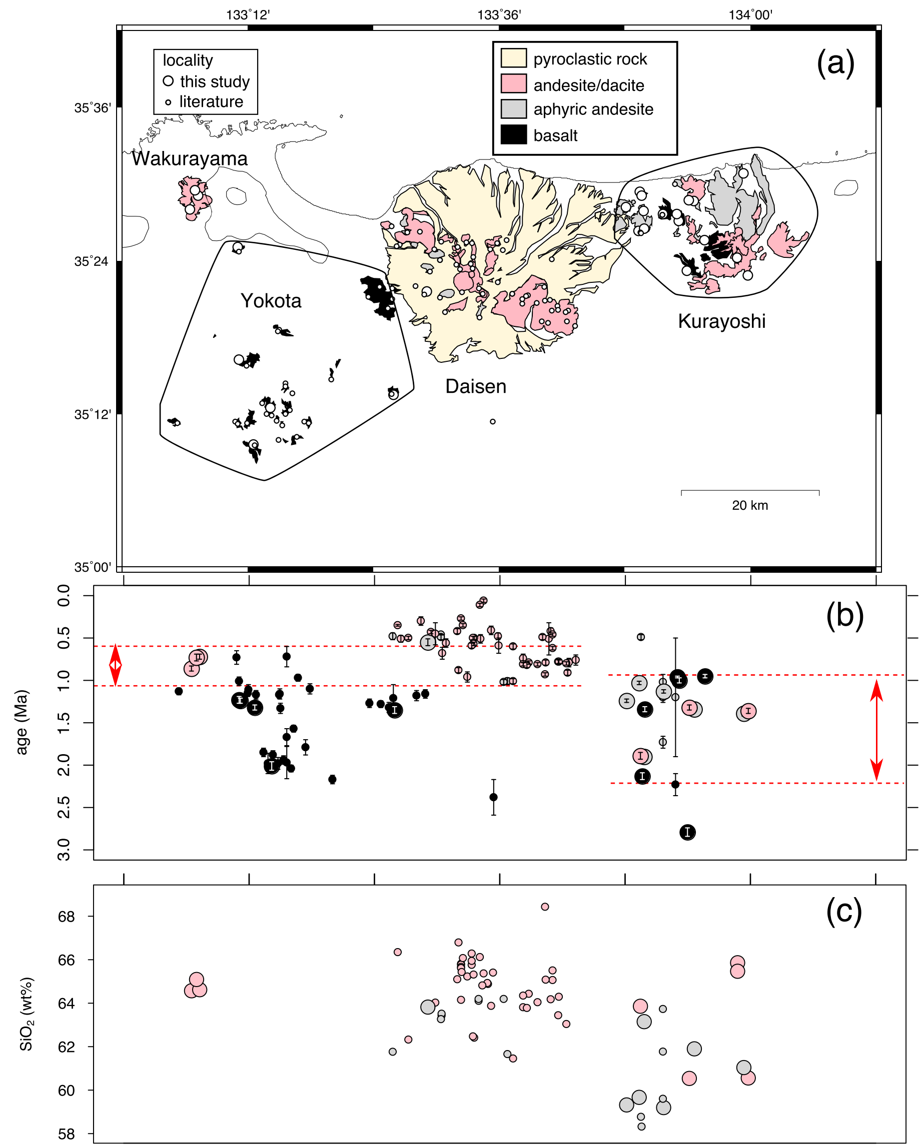

Figure 5. Distribution of high-Sr andesites and dacites and basalt lavas in Wakurayama, Yokota, Daisen, and Kurayoshi volcanic fields. (a) Occurrence of high-Sr andesites and dacites and other types of volcanic rocks and the locality of studied lavas. (b) Longitudinal variation in K-Ar age. The red arrows indicate the periods of concurrent activity of high-Sr andesites and dacites and basalts. The size of symbol denotes data source: large circle, this study (Tables S12 and S13); small circle, literature (Kimura et al., 2003; Tsukui et al., 1985; Uto, 1990; Tables S19 and S20). (c) Longitudinal variation in SiO_2 abundance of high-Sr andesite and dacite lavas. In (b) and (c), rock types are indicated by color: black, basalt; gray, high-Sr aphyric andesite; pink, high-Sr porphyritic andesite and dacite. Uncertainty on age is $1\sigma_m$.

In Kurayoshi volcanic field, andesites are dominant volumetrically. These lavas are associated with subordinate basaltic lavas (Figure 5; Murayama & Ozawa, 1961; Nagao & Nishikawa, 1980). Andesite lavas are classified as being aphyric or porphyritic, and the two types of lavas are commonly intercalated.

Southwest of the Daisen volcano, basaltic lavas are distributed sporadically in the Yokota region, with 20 volcanic centers with a 30 × 30-km geographic area. These lavas unconformably overlie the Cretaceous to Paleogene granites and Permian to Triassic metamorphic rocks (Hattori & Katada, 1964; Murayama, 1973).

2.4. The Other Regions

2.4.1. Himeshima

The Himeshima volcano consists of dacitic to rhyolitic lavas and pyrocloastic rocks (Itoh, 1990; Iwaya & Kurasawa, 1986), and basement is not exposed on the island on which this volcano is located. The volcanic activity is dated at 0.3–0.06 Ma by the fission track, K-Ar, and $^{40}Ar/^{39}Ar$ methods (Kamata et al., 1987; Kaneoka & Suzuki, 1970; Matsumoto et al., 2010).

2.4.2. Futagoyama, Yufu-Tsurumi, and Kuju in Hohi Volcanic Zone

The Hohi volcanic zone consists of 5,000 km^3 of volcanic rocks mostly andesite lavas and pyroclastic flow deposits. The basement includes Cretaceous granites and Paleozoic schist. The volcanic activity began at 5 Ma and continued to 0.3 Ma (Kamata, 1989), and adakitic signatures have been reported for andesitic to dacitic lavas from the Futagoyama, Yufu-Tsurumi, and Kuju volcanoes (Shibata et al., 2014; Sugimoto et al., 2006).

3. Samples

Andesite and dacite lavas were collected at the Aonoyama, Oe-Takayama, Sambe, Wakurayama, and Kurayoshi areas. They are classified as adakite, based on discrimination diagrams, with the exceptions of three samples from Aonoyama (Figure 2). These lavas are exposed near the other andesite and dacite lavas in Aonoyama and share petrological, chronological, geochemical, and isotopic features. Therefore, they are included in the Aonoyama high-Sr andesite-dacite suite. Basalt lavas and basement granitic rocks were also collected in the vicinity of the high-Sr andesite and dacite volcanic fields. Localities are shown in Figures 3–5, and their geodetic data are summarized in Tables S1–S10 in the supporting information.

4. Analytical Methods

All analyses were performed at the Pheasant Memorial Laboratory, Institute for Planetary Materials, Okayama University at Misasa (Nakamura et al., 2003). Rock samples were crushed with a jaw crusher to coarse chips of 3 to 5 mm in diameter. Fresh chips were carefully hand-picked and rinsed with deionized water in an ultrasonic bath. Chips for geochemical analyses were then dried at 100 °C for 12 hr and pulverized into powder using an alumina puck mill.

The K-Ar method was applied for dating volcanic rocks (Tables S11–S13). Chips were crushed to particles of 60–80 mesh (0.18–0.25 mm), and then the groundmass fraction was collected using a magnet separator. The abundance of radiogenic ^{40}Ar was determined by isotope-dilution mass spectrometry following the method of Nagao et al. (1996) and using a modified VG5400 mass spectrometer (Micromass, UK). Extraction and purification of Ar are described in Feyissa et al. (2017). Instrumental mass bias was corrected using the reference air with $^{40}Ar/^{36}Ar = 296.0$ (Nier, 1950). The abundance of K was determined by flame photometry using an AA-6200 (Shimadzu, Japan). Preparation of samples and instrumental calibration of K analysis are described in Feyissa et al. (2017). All analyses for K and Ar were duplicated. Relative difference of K concentration between duplicates is less than 1.5%, and the external reproducibility is estimated to be 2% (as 1σ). Decay constant of ^{40}K follows Steiger and Jäger (1977). During the course of the analyses, the reference standard rocks and minerals (ranging from 0.2 to 128 Ma) were analyzed along with samples. Our analyses yielded ages consistent with those reported in previous studies (Baksi et al., 1996; Nagao et al., 1996; Nakamura et al., 1986), thus confirming reliability of the method (Table S14).

Concentrations of major elements were determined by an X-ray fluorescence spectrometry with a Philips PW2400 instrument, using lithium tetraborate glass beads (with a 1:10 ratio of sample and flux), following the method of Takei (2002). Water content (H_2O^+) was obtained by gravimetric methods, and FeO wt % was determined by titration (Yokoyama & Nakamura, 2002). Trace element abundances were determined by inductively coupled plasma mass spectrometry using an Agilent 7500cs instrument, following the methods of Yokoyama et al. (1999), Makishima and Nakamura (2006), and Lu et al. (2007). Bomb decompositions were employed to ensure digestion of acid-resistant minerals such as zircon (Makishima et al., 2009), and all analyses were duplicated. Analytical reproducibilities (1σ) are 1% and 3–5% for major and trace element analyses, respectively.

Strontium, Nd, and Pb isotopic compositions were analyzed by thermal ionization mass spectrometry using a ThermoFisher TRITON, in a static multicollection mode. Instrumental mass bias during Sr and Nd isotope analyses was corrected using $^{86}Sr/^{88}Sr = 0.1194$ and $^{146}Nd/^{144}Nd = 0.7219$, respectively. For Pb isotope analyses, the normal double spike method of Kuritani and Nakamura (2003) was employed to correct instrumental mass bias. Acid leaching was performed in hot 6 M HCl (100 °C) for 8 hr, and the residual powders were multiply rinsed with deionized water prior to acid digestion. Procedures for column separations followed the methods of Yoshikawa and Nakamura (1993) for Sr, Nakamura et al. (2003) for Nd, and Kuritani and

10.1029/2017JB015066

Nakamura (2002) for Pb. During the course of the study, analyses of NIST SRM 987 yielded an average of $^{87}Sr/^{86}Sr$ = 0.710267 ± 0.000016 (2σ, *n* = 13), and the in-house standard (PML-Nd) yielded an average of $^{143}Nd/^{144}Nd$ = 0.511750 ± 0.000011 (2σ, *n* = 11), which corresponds to $^{143}Nd/^{144}Nd$ = 0.511886 for La Jolla (Marín-Cerón et al., 2010). The NIST SRM 987 and La Jolla data were renormalized to $^{87}Sr/^{86}Sr$ = 0.710240 and $^{143}Nd/^{144}Nd$ = 0.511860, respectively, and these normalization factors were applied to the sample data to facilitate comparison between data sets. The conversion factors of different reference standard materials (E&A $SrCO_3$, BCR-1, and JNdi-1) are taken from Gaffney et al. (2005), Weis et al. (2006), and Tanaka et al. (2000). The NIST SRM 981 Pb standard yielded an average of $^{206}Pb/^{204}Pb$ = 16.9429 ± 0.0014, $^{207}Pb/^{204}Pb$ = 15.4995 ± 0.0018, and $^{208}Pb/^{204}Pb$ = 36.7263 ± 0.0045 (2σ, *n* = 15); these values agree well with those obtained by Kuritani and Nakamura (2003). Analytical reproducibilities (2σ) are better than 30 ppm for Sr, 20 ppm for Nd, and 150 ppm for Pb, respectively. Geochemical data are summarized in Tables S1–S10.

5. Results

5.1. Petrography

5.1.1. High-Sr Andesites and Dacites

High-Sr andesites and dacites in the Chugoku district are divided into two types, aphyric and porphyritic, based on modal phenocryst composition (Figure S1 and Table S15 in the supporting information). The porphyritic type is found in all volcanic regions other than Wakurayama. Total phenocryst content ranges from 10 to 30 vol %, and euhedral to subhedral plagioclase is generally the most abundant (12–28 vol %). Some plagioclase exhibits dusty zones (Figures S1c and S1d), which are interpreted to have been formed by partial dissolution after crystallization (Tsuchiyama, 1985). Hornblende is the major mafic phase (2–12 vol %) and partly to completely replaced by opacite (Figures S1a–S1d). The lavas from the Aonoyama volcanic field are rich in hornblende (7–12 vol %) relative to the lavas from the other regions ($<$7 vol %) consistent with the relatively mafic composition of the whole rock samples. Quartz, orthopyroxene, biotite, and Fe-Ti oxides occur as minor phases (typically $<$3 vol %).

The aphyric type occurs in the Kurayoshi, Daisen, and Wakurayama volcanic fields (Sato et al., 2011; Tsukui, 1984). Total phenocryst abundance is less than 8 vol % (Table S15), consisting of plagioclase ($<$7 vol %) and microphenocrysts ($<$3 vol %) of orthopyroxene, hornblende (opacite), and Fe-Ti oxides (Figures S1e and S1f). Quartz occurs as rounded and corroded forms with reaction rims of pyroxene. The groundmass shows pilotaxitic texture, consisting mainly of plagioclase microlites.

5.1.2. Basalts

Basalt lavas, associated with the andesites and dacites, generally exhibit porphyritic texture (Figure S2 and Table S15). Euhedral to subhedral olivine is a ubiquitous phase (3–12 vol %) in all the lavas, typically with grain size up to 2 mm (see Figure S2). Olivine abundance is generally correlated with whole-rock MgO. Clinopyroxene, plagioclase, and Fe-Ti oxides occur at varying abundances (0–7 vol %). Some of the clinopyroxenes exhibit hourglass sector zoning. Groundmass is holocrystalline and shows intersertal texture, consisting mainly of plagioclase, pyroxene, and Fe-Ti oxides. Micas occur occasionally in cavities and groundmass interstitial.

5.2. Geochronology

Our data are combined with those obtained in the previous studies (Tables S16–S20), and the volcanic history in each region is described below.

5.2.1. Aonoyama and Abu

Latitudinal and longitudinal variations in K-Ar ages are shown in Figure 3. The ages of 1.3–1.0 Ma, reported for andesites and dacites from the north and central regions, date the onset of eruptions of this type of lava in Aonoyama (Kamata et al., 1987). At about 0.7 Ma, the volcanism became active in the entire region, ceasing at 0.3 Ma in the south and at ~0.1 Ma in the northern region. Basalt lavas from the Abu volcanic region yield K-Ar ages of 2.0 Ma to recent. As suggested in the previous studies (Kakubuchi et al., 2000; Koyaguchi, 1986), the volcanism is subdivided into two stages: 2.0–1.5 Ma (older series) and 0.8 Ma to present (younger series). The older and younger lavas occur near each other, showing no systematic spatial distribution (Figures 3b and 3c). Apparently, the eruptions of andesites and dacites occurred concurrently with basalts during the period of 0.8 Ma to recent (see the red arrow in Figure 3c).

5.2.2. Oe-Takayama, Sambe, and Mengame

Our K-Ar ages for Oe-Takayama dacites range from 1.9 to 1.0 Ma (Figure 4), consistent with the ages reported in previous studies (2.2–1.0 Ma, Kano et al., 2000; Kimura et al., 2003; Miura & Sawai, 2010; Sakoda et al., 2000). The dissected feature of Mt. Oe-Takayama is consistent with cessation of volcanism at 1 Ma.

The Sambe andesites and dacites yielded K-Ar ages ranging from 1.4 to $<$0.1 Ma. Volcanism in Sambe volcano presents a hiatus in its activity, dividing it in two stages (Kimura et al., 2003; Matsuura & Tsuchiya, 2003); the first stage yields from 1.4 to 1.0 Ma, and the second stage from 0.5 to $<$0.1 Ma (Figure 4b). In the older stage, low-Si andesites had erupted in the northern part of the volcano (Hattori et al., 1983; Matsuura & Tsuchiya, 2003). The younger lavas form the main volcanic body and are characterized by high-Si abundance (dacite; Figure 4c). We note that the cessation of eruption at Oe-Takayama is coincident with the onset of volcanic activity at Sambe, consistent with an eastward migration of the volcanic plumbing system (Figure 4b).

The basalt lavas from Mengame volcano, located 20 km southeast of Oe-Takayama and Sambe, yielded K-Ar ages of 1.05 and 1.11 Ma. With the K-Ar age of 1.8 ± 0.2 Ma for a basal lava (Matsuura, 1986), the volcanic activity had occurred during 1.8–1.0 Ma, concurrently with adakite eruptions in Oe-Takayama and Sambe (Figure 4b).

5.2.3. Wakurayama, Daisen, Yokota, and Kurayoshi

Three dacites from Wakurayama yield K-Ar ages of 0.9–0.7 Ma (Figure 5). Our new data reveal that the eruption of dacitic lavas at Wakurayama occurred concurrently with that of the other andesites and dacites in SW Japan. Previous studies reported older K-Ar ages of 6.3–5.0 Ma (Kawai & Hirooka, 1967; Morris et al., 1990) for samples referred to as "andesite," but descriptions of occurrences and petrologic and geochemical properties of these rocks were not presented. We infer that those older ages represent nonadakitic intermediate rocks from the basement of Wakurayama. The middle to late Miocene mafic to felsic rocks, termed the Matsue Formation, are distributed widely around Wakurayama (Kano et al., 1994; Morris & Itaya, 1997).

The K-Ar ages of Daisen andesites and dacites reported in Tsukui et al. (1985) and Kimura et al. (2003) range from 1.0 to 0.1 Ma. We also obtained the age of 0.55 Ma for an aphyric andesite in the western part of Daisen. Spatial distribution of the compiled ages (Figure 5b) shows that the volcanism shifted from southeast to northwest during 1–0.5 Ma, with no systematic spatial and temporal variations in lava type (Figure 5c). In the ensuing period ($<$0.5 Ma), the activity had declined, ceasing at 18–17 ka with eruptions of pyroclastic fall deposits (^{14}C ages for carbonized wood and fossils in ash layers; Domitsu et al., 2002; Yamamoto, 2017).

The Yokota basalts yielded K-Ar ages of 2.0–1.2 Ma (Figure 5). With younger ages (1–0.7 Ma) for the other flows (Kimura et al., 2003; Uto, 1990), the duration of volcanism is estimated to be 1.3 Myr. Concentric zoning is observed in the spatial distribution of ages (Kimura et al., 2003): 2–0.5 Ma in the central region and $<$1.2 Ma in the peripheral regions. The duration of basalt eruptions overlaps with that of the eruptions of andesites and dacites in Wakurayama and Daisen for 1.0–0.6 Ma (see the red arrows in Figure 5b).

The andesite lavas in Kurayoshi yielded K-Ar ages of 1.9–1.0 Ma (Figure 5b), consistent with results of previous studies (Kimura et al., 2003; Tsukui et al., 1985; Uto, 1990). The ages of two different types of andesites (aphyric and porphyritic types) strongly overlap each other. The eruptions of basalt lavas began at 2.8 Ma and continued to 1 Ma. Eruptions of basalt and andesite magmas had occurred concurrently during the period between 2.3 and 1.0 Ma (Figure 5b).

5.3. Major Elements

A compositional gap is present at SiO_2 = 55–58 wt %, dividing the rocks into basalt and andesite-dacite series (the latter series are denoted as high-Sr andesites or dacites). This bimodal feature is pronounced by comparison of major-element compositions with Quaternary volcanic rocks in NE Japan arc (Figure 6). The andesites and dacites in SW Japan are classified into subalkaline series, as they plot below the boundary line of alkaline and subalkaline series in a total alkali ($Na_2O + K_2O$)-SiO_2 diagram (Figure 6; Kuno, 1966). They are also classified into the medium-K series on a K_2O-SiO_2 diagram (Le Maitre et al., 1989). The Aonoyama, Sambe, Daisen, and Kurayoshi volcanic fields include both andesite and dacite. In the Daisen and Kurayoshi volcanic fields, porphyritic lavas tend to be more differentiated (enriched in SiO_2) than aphyric lavas. The Oe-Takayama and Wakurayama lavas show homogeneous SiO_2 and do not include andesite. Overall, these lavas show increases in Na_2O and K_2O and decreases in TiO_2, Al_2O_3, FeO^T (total Fe as FeO), MnO, MgO, CaO, and P_2O_5 with increasing SiO_2.

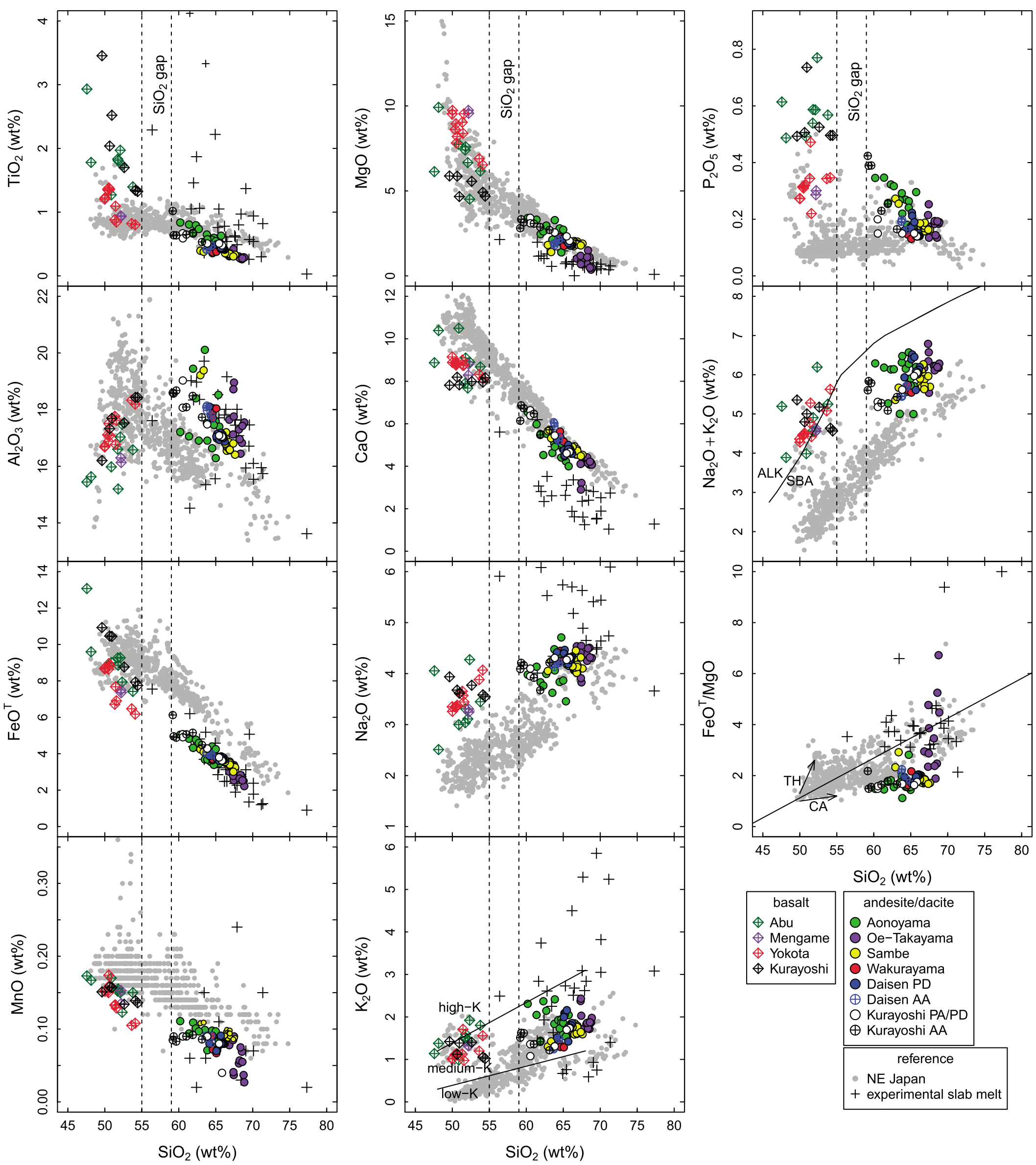

Figure 6. Major-element variation diagrams. Abundances of total oxides are normalized to 100% volatile free. Data for Daisen volcanic rocks are from Feineman et al. (2013). PD, porphyritic dacite; AA, aphyric andesite; PA, porphyritic andesite. Compositions of experimental slab melts are from Rapp et al. (1991), Sen and Dunn (1994), Rapp (1995), and Pertermann and Hirschmann (2003). The boundary lines for low-/medium-/high-K series and alkaline (ALK)-/subalkaline (SBA) series are after Le Maitre et al. (1989) and Kuno (1966), respectively. The reference slope for discrimination of tholeiitic (TH) and calc-alkaline (CA) series is from Miyashiro (1974). The reference data for Quaternary volcanic rocks from NE-Japan arc are summarized in Table S37 (Ban & Yamamoto, 2002; Fujinawa, 1988, 1992; Hunter & Blake, 1995; Kimura & Yoshida, 2006; Kimura et al., 2002; Kudo et al., 2007; Kuritani, Yoshida, Kimura, Hirahara, et al., 2014; Moriguti et al., 2004; Ohba et al., 2009; Sakuyama & Nesbitt, 1986; Takahashi et al., 2013; Tatsumi et al., 2008; Toya et al., 2005; Ueki & Iwamori, 2017; Yamamoto, 1988).

Compared with andesite-dacite-rhyolite (ADR) suite in NE Japan arc, the andesites and dacites in the Chugoku district have higher Al_2O_3, Na_2O, and total alkali contents and lower FeO^T and MnO contents (Figure 6). The majority of these andesites and dacites form the SiO_2-enrichment trend with smaller change in FeO^T/MgO and thus are classified as calc-alkaline series (Miyashiro, 1974). The exception is the Oe-Takayama lavas showing highly variable FeO^T/MgO at a constant SiO_2. The FeO contents (determined by titration) of the Oe-Takayama lavas positively correlate with MgO contents, whereas the Fe_2O_3 contents do not vary with change in MgO (Figure S3). The variations in Fe_2O_3, FeO, and MgO are attributed to variable modal abundance of hornblende (Hb) and iron oxides (Ox). The Hb dominates Fe^{2+} and Mg, while the latter holds the most Fe^{3+}. The rocks with anomalously high FeO^T/MgO contain fewer Hb phenocrysts but contain

10.1029/2017JB015066

Fe oxides (Ox) as phenocryst and groundmass phases in amounts similar to the other lavas. Owing to low Fe and Mg contents of Oe-Takayama lavas, the Hb/Ox ratio significantly changes Fe^{2+}/Fe^{3+} ratio as well as Mg content of whole rocks, resulting in large variation of FeO^T/MgO. Sato et al. (2011) also found the similar but more various FeO^T/MgO (2–14) for Wakurayama dacites based on larger number of sample set. The mafic phases in these lavas are also dominated by Hb, and its modal abundance is variable.

The basaltic lavas have SiO_2 = 46–55 wt %. Compared with typical island arc basalts (Perfit et al., 1980), they have relatively high abundances of Na_2O and K_2O and thus are transitional to alkaline basalt or medium-K to high-K series. Less differentiated lavas ($FeO^T/MgO < 1$) occur in the Abu, Mengame, and Yokota volcanic fields.

5.4. Trace Elements

Figures 7 and 8 highlight the trace element features of the andesites and dacites in the Chugoku district which are distinctly different from those of the Quaternary ADR lavas in NE Japan. The andesites and dacites in this district are enriched in Sr and light rare earth elements (REEs) and depleted in Y and heavy REE at various extent (Figures 7 and 8). The Aonoyama andesites and dacites have the lowest $(La/Yb)_n$ among those in the Chugoku district, with a mean of 12.8 ± 3.8 (subscript n denotes chondrite normalized abundance). The Oe-Takayama and Sambe andesites and dacites have higher $(La/Yb)_n$: 32.4 ± 9.5 for the former and 21.1 ± 2.2 for the latter. The andesites and dacites from Wakurayama, Daisen, and Kurayoshi have the intermediate La/Yb. The porphyritic and aphyric andesites and dacites in Daisen and Kurayoshi show similar REE patterns. Plots of Sr and Y against SiO_2 suggest that variations in Sr/Y (and light REE/heavy REE) mainly reflect variation in Sr (and light REE; Figure 8). The basaltic lavas generally have higher REE abundance and lower light-to-heavy-REE ratios than those of andesites and dacites with which they are associated.

The volcanic rocks in the Chugoku district show the covariations of trace element compositions with SiO_2 and Mg# [$\equiv$Mg/(Mg + Fe^{2+})], which are distinctly different from the Quaternary volcanic rocks in NE Japan (Figure 8). The abundances of Sr in the Chugoku district volcanic rocks (~600–2,200 $\mu g\ g^{-1}$) are $>$3 times higher than the NE-Japan volcanic rocks (mostly $<$300 $\mu g\ g^{-1}$). The abundances of Y in the Chugoku-district volcanic rocks decrease with increasing SiO_2, whereas the NE-Japan volcanic rocks show increasing abundance of Y with increasing SiO_2. The features of the volcanic rocks in the Chugoku district are similar to andesites and dacites in the western Aleutian arc (Yogodzinski et al., 2015, 2017). The element ratios highlight geochemical signatures of the volcanic rocks in the Chugoku district differing from the NE-Japan volcanic rocks. Also noted are the elevating Sr/Y and La/Yb ratios with decreasing Mg# (0.60–0.25). This feature is different from the western Aleutian ADR which shows large variations in Sr/Y and La/Yb for a limited Mg# (0.65–0.50; Yogodzinski et al., 2015).

High-Sr andesites and dacites show enrichments in large-ion lithophile elements (Cs, Rb, Ba, and K), Pb, Sr, and Li, and depletions in Nb and Ta, when plotted on an N-MORB-normalized diagram (Figure S4, trace elements abundance of N-MORB after Gale et al., 2013; Ryan et al., 1996). Such features are typical of island arc volcanic rocks (Shibata & Nakamura, 1997; Yokoyama et al., 2003). High-Sr andesites and dacites possess positive Zr and Nb anomalies, rare in island arc magmas but found occasionally in volcanic rocks from rear-arc regions (Kuritani et al., 2008). The basaltic lavas also exhibit enrichments of large-ion lithophile elements, Pb, Sr, and Li. Niobium and Ta show varying extent of enrichment; the Mengame and Yokota lavas show negative Nb-Ta anomalies, whereas the Abu and Kurayoshi lavas do not exhibit such anomalies (except for shoshonite in Abu, which show strong depletion of Nb and Ta; Kimura et al., 2014).

5.5. Isotopes

New Sr, Nd, and Pb isotope data for high-Sr andesites and dacites and basalts in the Chugoku district are plotted in Figures 9 and 10, along with previously published data sets for high-Sr andesites and dacites from Aonoyama and Daisen (Feineman et al., 2013; Kimura et al., 2014; Pineda-Velasco et al., 2015). Broad negative arrays are formed in Sr-Nd and Pb-Nd isotope plots (Figures 9a, 9b, 9e, and 9f), whereas a broad positive array is formed in Pb-Sr plot (Figures 9c and 9d). The $^{87}Sr/^{86}Sr$ and $^{143}Nd/^{144}Nd$ of high-Sr andesites and dacites in the Chugoku district largely overlap with those of ADR suite in NE Japan (Figure 9b). The Aonoyama lavas have the most radiogenic and more variable $^{143}Nd/^{144}Nd$ (0.51284–0.51293) and the least radiogenic and

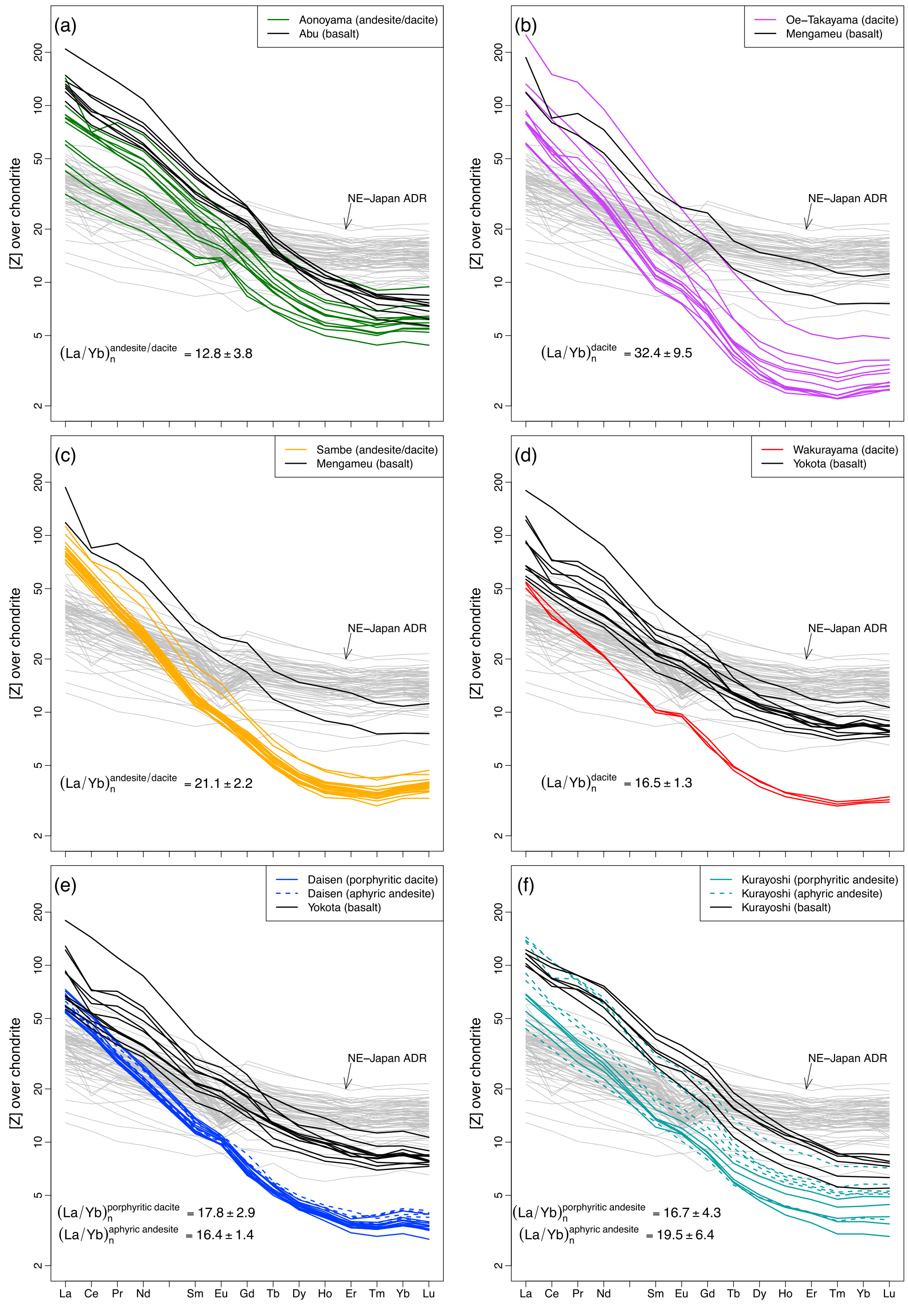

Figure 7. Chondrite-normalized rare earth element abundances of andesites and dacites and associated basalts: (a) Aonoyama and Abu; (b) Oe-Takayama and Mengame; (c) Sambe and Mengame; (d) Wakurayama and Yokota; (e) Daisen (PD, porphyritic dacite; AA, aphyric andesite) and Yokota; and (f) Kurayoshi (PA/PD, porphyritic andesite and dacite; AA, aphyric andesite). Data for Daisen volcanic rocks are from Feineman et al. (2013). Data for Quaternary andesite-dacite-rhyolite suite (ADR, $SiO_2 > 57$ wt % anhydrous basis) in NE Japan (fore-arc volcanoes) are summarized in Table S36 (Fujinawa, 1988, 1992; Kimura & Yoshida, 2006; Kimura et al., 2002; Kuritani, Yoshida, Kimura, Takahashi, et al., 2014; Moriguti et al., 2004; Ohba et al., 2009; Takahashi et al., 2013; Tatsumi et al., 2008). Element abundances of chondrite are from Boynton (1983).

less variable $^{87}Sr/^{86}Sr$ (0.70343–0.70351; Kimura et al., 2014), whereas Sambe, Daisen, and Kurayoshi andesites and dacites have more radiogenic and variable $^{87}Sr/^{86}Sr$ (0.7041–0.7056; Feineman et al., 2013; Kimura et al., 2014, this study). Consequently, the andesites and dacites from Aonoyama and other volcanic fields form the Sr-Nd isotope arrays with different slopes (Figures 9a and 9b). The associated basalts have the compositions which overlap partially with and more variable than those of the andesites and dacites ($^{87}Sr/^{86}Sr$ = 0.7035–0.7068, $^{143}Nd/^{144}Nd$ = 0.51248–0.51284; Figure 9a).

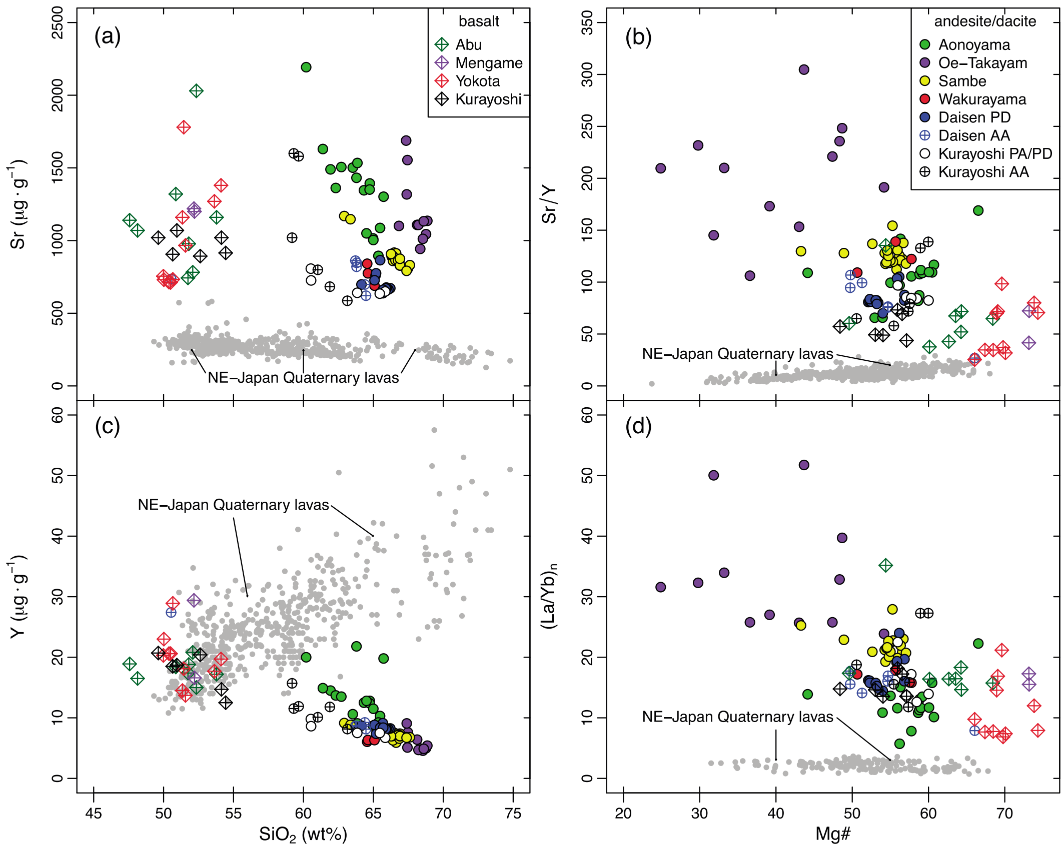

Figure 8. Covariations between (a) SiO_2 and Sr, (b) SiO_2 and Y, (c) Mg# [≡Mg/(Mg + Fe^{2+})] and Sr/Y, and (d) Mg# and $(La/Yb)_n$ for the volcanic rocks in the Chugoku district. Data for NE-Japan Quaternary lavas (fore-arc volcanoes) are summarized in Tables S35–S37 (Ban & Yamamoto, 2002; Hunter & Blake, 1995; Kimura et al., 2002; Kimura & Yoshida, 2006; Kudo et al., 2007; Kuritani, Yoshida, Kimura, Hirahara, et al., 2014; Kuritani, Yoshida, Kimura, Takahashi, et al., 2014; Moriguti et al., 2004; Ohba et al., 2009; Sakuyama & Nesbitt, 1986; Takahashi et al., 2013; Tatsumi et al., 2008; Toya et al., 2005; Ueki & Iwamori, 2017).

The Pb isotopic compositions of high-Sr andesites and dacites in the Chugoku district are less radiogenic ($^{206}Pb/^{204}Pb$ = 18.054–18.337, Figures 10a and 10c) and little overlap with those of ADR suite in NE Japan (Figures 9d, 9f, 10b, and 10d). Among the andesites and dacites in the Chugoku district, Aonoyama lavas have the least radiogenic and more variable Pb-isotopic composition ($^{206}Pb/^{204}Pb$ = 18.054–18.217). The andesites and dacites from the other volcanic fields have more radiogenic and homogeneous compositions ($^{206}Pb/^{204}Pb$ = 18.205–18.337). The associated basalts have the compositions which overlap partially with and extend to more radiogenic than those of the andesites and dacites.

Our new data confirm that the high-Sr andesites and dacites in SW Japan share the common Pb-isotope linear trend (Figures 10b and 10d) suggested by Pineda-Velasco et al. (2015). The less radiogenic extension points toward the composition of sea-floor basalts from the Shikoku Basin (Hickey-Vargas, 1991, 1998; Ishizuka et al., 2009; Straub et al., 2010), whereas the radiogenic extension is toward the compositions of sediment in Nankai Trough (Ishikawa & Nakamura, 1994; Plank & Langmuir, 1998; Shimoda et al., 1998; Tables S21, S22, and S23).

6. Discussion

6.1. Origin of High-Sr Andesite and Dacite

Since the first finding of adakite (i.e., high-Sr andesite and dacite) as products of slab melting (Defant & Drummond, 1990; Kay, 1978), increasing numbers of rocks of this type have been reported from various tectonic settings, leading to alternative models involving (1) high-pressure fractional crystallization of arc basalts (Alonso-Perez et al., 2009; Macpherson et al., 2006; Ribeiro et al., 2016) and (2) partial melting of

10.1029/2017JB015066

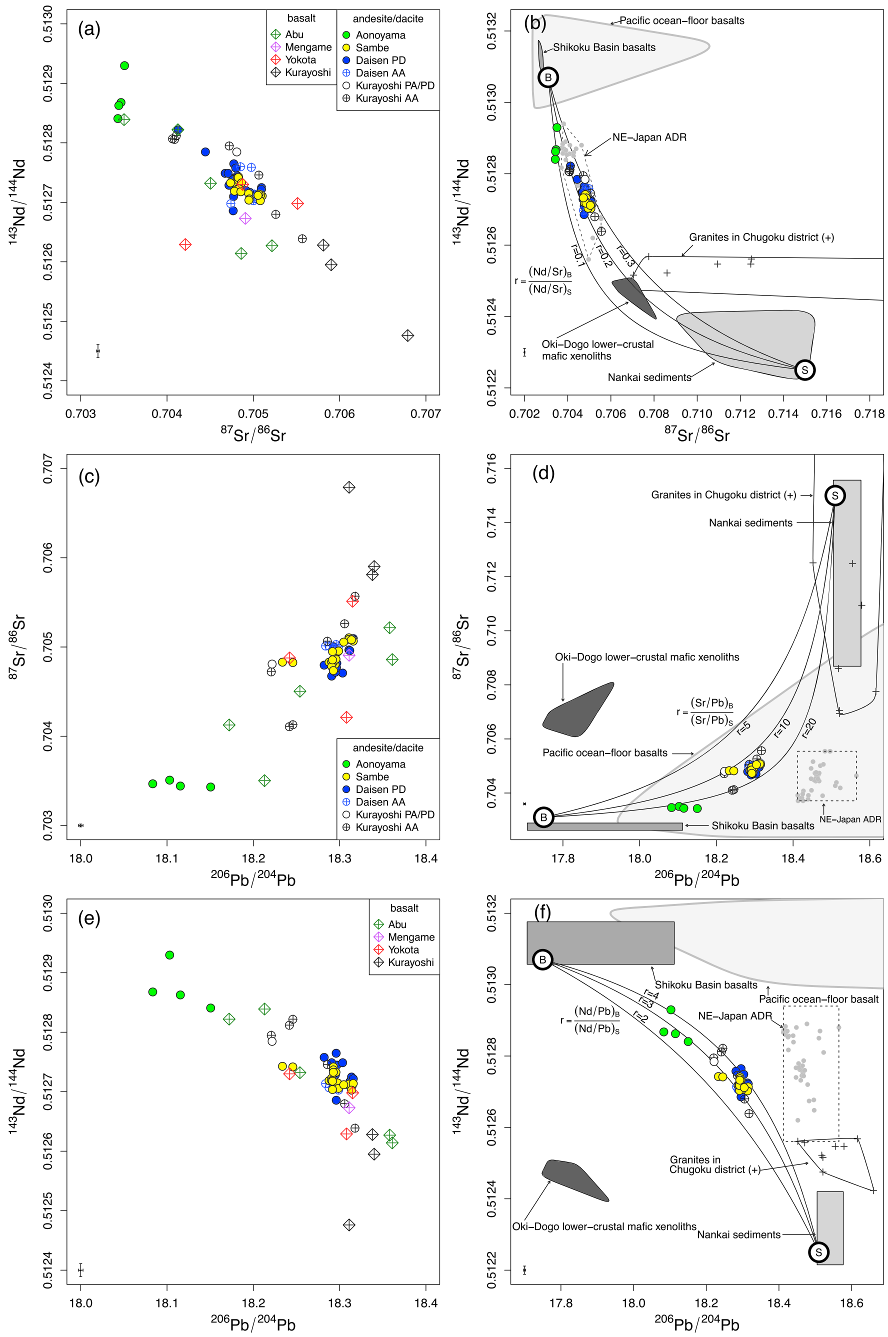

Figure 9. Plots of Sr-Nd-Pb isotope compositions for the volcanic rocks in Chugoku district. (a and b) $^{87}Sr/^{86}Sr$ versus $^{143}Nd/^{144}Nd$, (c and d) $^{206}Pb/^{204}Pb$ versus $^{87}Sr/^{86}Sr$, and (e and f) $^{206}Pb/^{204}Pb$ versus $^{143}Nd/^{144}Nd$. Data for andesites and dacites from Daisen and Aonoyama volcanic fields are from Feineman et al. (2013) and Kimura et al. (2014), respectively. The compositional variations for subducting basalts, sediments, and lower and upper crustal rocks are shown as gray-scaled fields: Shikoku Basin basalts (Hickey-Vargas, 1991, 1998; Ishizuka et al., 2009; Straub et al., 2010; Table S21), Nankai sediments (Shimoda et al., 1998; Terakado et al., 1988; Table S22), Pacific Ocean-floor basalts (Castillo et al., 1992; Hauff et al., 2003; Janney & Castillo, 1997; Table S38), late Cretaceous to early Paleogene granites in Chugoku district (Feineman et al., 2013, this study; Table S10), and lower-crustal mafic xenoliths from Oki-Dogo (Moriyama, 2006). Data for Quaternary andesite-dacite-rhyolite suite ($SiO_2 > 57$ wt % anhydrous basis) in NE Japan (fore-arc volcanoes) are shown by gray dots enclosed with a dash line. Data are summarized in Table S39 (Kimura & Yoshida, 2006; Kuritani, Yoshida, Kimura, Takahashi, et al., 2014; Moriguti et al., 2004; Takahashi et al., 2013; Tatsumi et al., 2008). The hyperbolic curves shown in Figures 9b, 9d, and 9f are those for mixing of components from subducting basalt (denoted as "B") and sediment ("S") with various r [$=(Nd/Sr)_B/(Nd/Sr)_S$ of 0.1–0.3 or $(Sr/Pb)_B/(Sr/Pb)_S$ of 5–20 or $(Nd/Pb)_B/(Nd/Pb)_S$ of 2–4]. Analytical uncertainty (22 ppm for Sr, 21 ppm for Nd, and 150 ppm for Pb) is shown as error bar on the lower-left side.

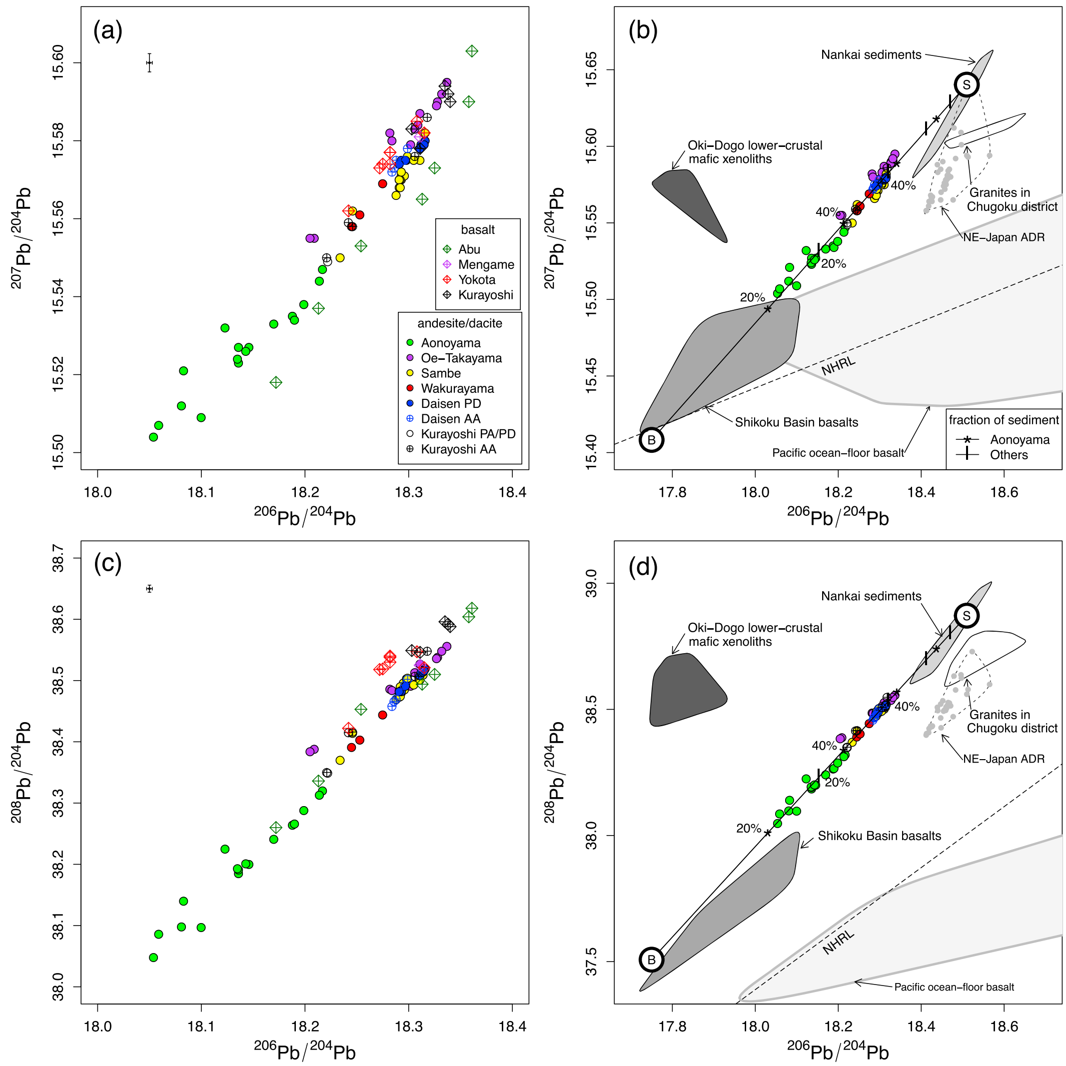

Figure 10. Plots of Pb-isotope compositions. (a and c) $^{206}Pb/^{204}Pb$ versus $^{207}Pb/^{204}Pb$ and $^{208}Pb/^{204}Pb$ of andesites, dacites, and basalts in Chugoku district, SW Japan. (b and d) $^{206}Pb/^{204}Pb$ versus $^{207}Pb/^{204}Pb$ and $^{208}Pb/^{204}Pb$ of andesites and dacites in Chugoku district in comparison with Shikoku Basin basalts (Hickey-Vargas, 1991, 1998; Ishizuka et al., 2009; Straub et al., 2010; Table S21), Nankai sediment (Ishikawa & Nakamura, 1994; Shimoda et al., 1998; Table S22), Pacific Ocean-floor basalts (Castillo et al., 1992; Hauff et al., 2003; Janney & Castillo, 1997; Table S38), late Cretaceous to early Paleogene granites in Chugoku district (Feineman et al., 2013, this study; Table S10), lower continental mafic xenoliths from Oki-Dogo (Moriyama, 2006). Data for Quaternary andesite-dacite-rhyolite suite ($SiO_2 > 57$ wt % anhydrous basis) in NE Japan (fore-arc volcanoes) are shown by gray dots enclosed with a dash line. Data are summarized in Table S39 (Kimura & Yoshida, 2006; Kuritani, Yoshida, Kimura, Takahashi, et al., 2014; Moriguti et al., 2004; Takahashi et al., 2013; Tatsumi et al., 2008). Also shown are the lines for mixing of components from subducting basalt (denoted as "B") and sediment ("S"). The dashed lines in (b) and (d) are Northern Hemisphere Reference Line (Hart, 1984). Analytical uncertainty is shown as error bar (150 ppm) on the upper-left side in (a) and (c).

mafic lower crust (Atherton & Petford, 1993; Gao et al., 2004; Xu et al., 2002). Below we discuss the applicability of these alternatives for the origin of high-Sr andesites and dacites in the SW Japan arc.

6.1.1. High-Pressure Fractional Crystallization of Basalt in the Lower Crust

High-pressure experiments (Alonso-Perez et al., 2009; Müntener & Ulmer, 2006) demonstrated that subalkaline basaltic to andesitic melts have garnet as a liquidus phase under pressure (*P*) of 0.8–1.5 GPa, corresponding to lower-crustal depth in SW Japan (~30–40 km; Katsumata, 2010; Yamane et al., 2012). Accordingly, the high-Sr andesite and dacite magmas with "garnet signature" can be produced by fractional crystallization of parental basalt magmas at the base of the crust (Zellmer et al., 2012). However, it is unlikely that the process is solely responsible for the genesis of high-Sr andesites and dacites in SW Japan, for the following reasons: (1) crystallization of the other phases observed in experimental and natural samples (olivine, clinopyroxene, spinel, hornblende, and plagioclase) produces differentiated magmas with higher light REE abundances and lower heavy REE abundances compared to those of basaltic lavas (see also Kimura et al., 2014 in which this issue is examined in detail by crystallization model); however, such features are not documented by the patterns shown in Figure 7, and (2) Pb isotopic compositions of high-Sr andesites and dacites and associated basalts show significant variations, also suggesting that basalt and andesite-dacite magmas were originated from different source rocks (Figures 10a and 10c).

6.1.2. Partial Melting of Mafic Lower Crust

Magmatic underplating has been considered a major process in the formation of the lower crust. Mantle-derived magmas intrude into the mantle-crust boundary and crystallize to form mafic lower crust (Arndt & Goldstein, 1989). Melting experiments demonstrated that andesite to dacite magmas can be produced by melting of such mafic lower crust (at 1.0–1.5 GPa and 800–1,000 °C; Qian & Hermann, 2013; Springer & Seck, 1997); thus, the pressure and temperature (*P*–*T*) condition at the depth of the lower crust (0.8–1.5 GPa, 800–1,050 °C) can lead to melting of mafic rocks (Nozaka, 1997; Takahashi, 1978). The possible contribution of lower crust to the lavas studied here was examined using Pb isotope compositions of mafic xenoliths (gabbro and pyroxenite) from Oki-Dogo (Moriyama, 2006) located 90 km north of Daisen (Figure 1). The involvement of two magma sources is suggested for the genesis of high-Sr andesites and dacites from a linear array in $^{206}Pb/^{204}Pb$–$^{207}Pb/^{204}Pb$ and $^{206}Pb/^{204}Pb$–$^{208}Pb/^{204}Pb$ plots (Figures 10b and 10d). On the plots, the magma source compositions can be estimated by extrapolation of a linear array (denoted as the circles labeled “B” and “S”). Neither of them have the composition consistent with the lower crustal rocks in SW Japan. We therefore ruled out the lower crustal melting as having produced the high-Sr andesites and dacites.

6.1.3. Partial Melting of Subducted Slab

The high-Sr andesites and dacites in SW Japan arc show geochemical features consistent with adakite as defined by Defant and Drummond (1990): high SiO_2 (≥56 wt %) and Al_2O_3 (≥15 wt %) and low MgO (<3 wt %). They also have major-element compositions comparable to experimental slab melts (Figure 6). The slab-melt origin is also supported by spatial distribution of volcanoes; they are well aligned along the 80 to 100-km contours of subducting Shikoku Basin Plate (Figure 1). At that depth, the igneous layer of the slab metamorphoses to eclogite-facies rocks consisting dominantly of clinopyroxene and garnet (Poli & Schmidt, 2002). Melting experiments documented that, at that depth, eclogitic rocks can form intermediate to felsic melts leaving garnet-bearing residues under both hydrous and anhydrous conditions (Pertermann & Hirschmann, 2003; Rapp, 1995; Rapp et al., 1991; Sen & Dunn, 1994). In summary, the occurrence and geochemical characteristics of high-Sr andesites and dacites in Chugoku district, SW Japan, are best explained by melting of the subducting Shikoku Basin Plate.

6.2. Crustal Assimilation

The $^{87}Sr/^{86}Sr$ ratios of the high-Sr andesites and dacites in SW Japan range from 0.7034 to 0.7056 (Figure 9) and are in general more radiogenic than those for typical adakites (<0.7040; Defant & Drummond, 1990). Such a feature could be attributed to (1) crustal assimilation during magma ascent (Kimura et al., 2014) or (2) sediment contribution to magma sources (Feineman et al., 2013).

The assimilation of crustal materials is unlikely to explain radiogenic $^{87}Sr/^{86}Sr$ because the magmatic temperature (~900 °C; Tamura et al., 2003; Tsukui, 1985) is likely to have been too low to result in ingestion of significant quantities of granitic country rocks (melting points ~950 °C; Grove et al., 1988). The insignificant role of crustal assimilation is also evident on the $^{207}Pb/^{204}Pb$–$^{206}Pb/^{204}Pb$ and $^{208}Pb/^{204}Pb$–$^{206}Pb/^{204}Pb$ plots (Figure 10). The linear array in the plots points toward two end-member components clearly distinct in composition from the upper and lower crustal materials (granites and mafic xenoliths, respectively). Thus, we conclude that crustal assimilation did not play a major role in the genesis of high-Sr andesites and dacites in SW Japan. Instead, we propose that the radiogenic Pb isotopic composition can be attributed to the involvement of sediment, as was first proposed by Feineman et al. (2013).

6.3. Sediment Contribution

Feineman et al. (2013) attributed high $^{87}Sr/^{86}Sr$ ratios of andesites and dacites from Daisen volcanic field to significant contribution from subducted sediments. We examine the role of sediments in the genesis of high-Sr andesites and dacites using geochemical and isotope data sets for the lavas from the other volcanic fields obtained in this study and the other published studies (Kimura et al., 2014, 2015; Pineda-Velasco et al., 2015). Linear arrays in $^{206}Pb/^{204}Pb$–$^{207}Pb/^{204}Pb$ and $^{206}Pb/^{204}Pb$–$^{208}Pb/^{204}Pb$ plots (Figure 10) are consistent with

10.1029/2017JB015066

mixing of two-end member components derived from subducting basalt and sediment (denoted as the circles with "B" and "S," respectively). The broad negative correlation in $^{87}Sr/^{86}Sr$ versus $^{143}Nd/^{144}Nd$ plot (Figure 9) also reinforces the involvements of these two end-member components.

As noted by Kimura et al. (2014), the Aonoyama lavas form the nearly vertical trend in an $^{87}Sr/^{86}Sr$–$^{143}Nd/^{144}Nd$ plot (Figures 9a and 9b), whereas the other andesites and dacites form the shallower trend. The difference in slopes in the plot can ascribe to difference in Nd/Sr ratios of two end-member components. It is the most likely that the basalt component in Aonoyama lavas has lower Nd/Sr ratio than that contributed to the other lavas, probably due to lower degree of melting ($D_{Sr}^{eclogite/melt} < D_{Nd}^{eclogite/melt}$, Table S24). To substantiate this inference, a general mixing equation (Langmuir et al., 1978) is applied to Sr-Nd, Pb-Sr, and Pb-Nd isotope mixing (Figure 9). The curvature function *r* is used to examine the difference in melting degree of the subducting basalt; *r* is defined as $(Nd/Sr)_B/(Nd/Sr)_S$ for an Sr-Nd isotope plot, $(Sr/Pb)_B/(Sr/Pb)_S$ for an Sr-Pb isotope plot, and $(Nd/Pb)_B/(Nd/Pb)_S$ for a Pb-Nd isotope plot, respectively. The Aonoyama data fit well with hyperbolic curves for Sr-Nd isotope mixing with smaller *r*, and that for Pb-Sr isotope mixing with greater *r*, compared with other andesites and dacites. This result is consistent with various melting degree of the subducting basalt and also supported by the variation in volume of lavas (smaller degree of melting for Aonoyama; Kimura et al., 2014).

The mixing modeling also places constrains on the end-member compositions. The less radiogenic extension of Sr-Nd isotope mixing curve points to $^{87}Sr/^{86}Sr$ of 0.7031 for the subducting basalt, which is significantly lower than that estimated for the subducting basalt of Pacific Plate in the Aleutian arc (0.7036–0.7050, Yogodzinski et al., 2017) and seemingly consistent with young age of the Shikoku Basin Plate (26–15 Ma, Okino et al., 1994). In the following sections, we discuss (1) mass balance of sediment and oceanic crust and (2) the lateral variations in sediment flux in the high-Sr andesites and dacites.

6.3.1. Mass Balance

We examine trace element concentrations of slab- and sediment-derived melts using a modal batch melting (Shaw, 1970). The composition of subducting basalt is taken from sea-floor basalt in Shikoku Basin (Tables S21 and S23; Hickey-Vargas, 1991, 1998; Ishizuka et al., 2009; Straub et al., 2010), and the sediment composition is that from Nankai Trough (Tables S22 and S23; Ishikawa & Nakamura, 1994; Plank & Langmuir, 1998; Shimoda et al., 1998, 2003; Terakado et al., 1988). Partition coefficients between melt and residues are shown in Table S24 (Johnson & Plank, 1999 and Kelemen et al., 2003 with source mode of Rapp & Watson, 1995), and calculated trace element concentrations of partial melts at various degree of melting (*F*) are summarized in Table S25.

The calculated melt compositions of sediment and basaltic crust show variations with change in *F*. The *F* for sediment is estimated to be 30% following Feineman et al. (2013), whereas that for subducting basalt is estimated using the *r* values of hyperbolic mixing curves in Sr-Nd-Pb isotope plots (Figure 9) with Nd/Sr, Pb/Sr, and Pb/Nd ratios of sediment melt. We obtained *F* of 5% for Aonoyama lavas and 15% for the other lavas, consistent with the previous studies (Feineman et al., 2013; Kimura et al., 2014).

Relative contributions of subducted basalt- and sediment-derived components were examined by mass balance modeling using the calculated trace element concentrations and measured Pb-isotopic compositions. Mixing of 20–45% sediment component with 55–80% basalt component generally reproduces the observed trace element and Pb-isotope compositions of high-Sr andesites and dacites (Figures 10 and S5). The mass fraction of sediment obtained in this study is essentially identical to that calculated by Feineman et al. (2013). The Aonoyama rocks and Daisen aphyric andesites show enrichments of heavy REE compared with the modeled melts (Figures 7 and S5 and Table S26), and the possible causes are discussed in section 6.4.

6.3.2. Implications for Transportation

Sediment contribution to each volcanic field is examined using key trace element ratios and Pb-isotope composition (Figure 11). Plots of Th/Nb and Pb/Nd show the longitudinal variations similar to that of mass fraction of sediment estimated by Pb-isotope mixing model (Figure 10). These proxies do not show systematic along-arc variations, suggesting that subducted sediment contributed in a significant amount in the broad area in this volcanic arc. A larger contribution of sediment is attributed to the combined effects of sedimentation and seamount subduction.

Sediments accumulate to a greater extent in the Shikoku Basin due to high turbidite drainage and sedimentation facilitated by roughness of basement relief (Ike et al., 2008; Figure 1). It is also noted that the Shikoku

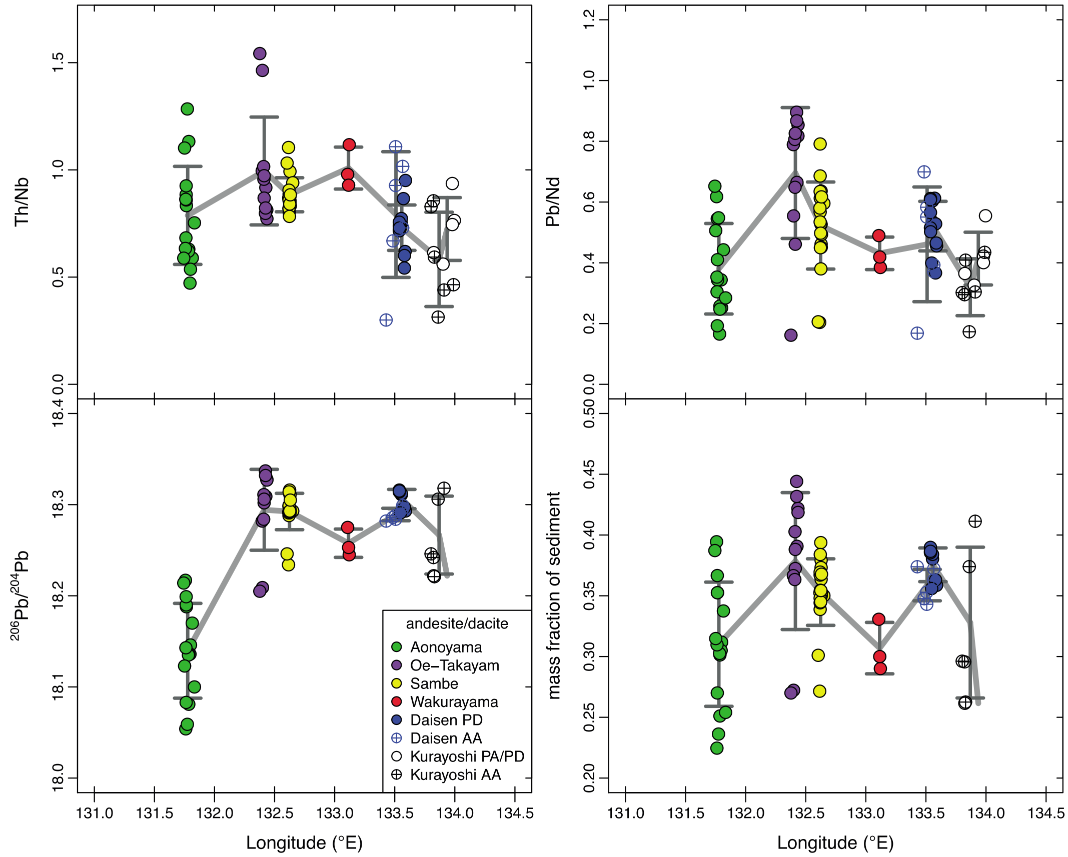

Figure 11. Longitudinal variations in Th/Nb, Pb/Nd, $^{206}Pb/^{204}Pb$, and mass fraction of sediment (estimated in Figure 10) of high-Sr andesites and dacites in the Chugoku district, southwest Japan. The mean values in each volcanic field are connected by thick gray lines. The error bars on each mean indicate 1σ variation within each volcanic field.

Basin Plate has two prominences, Kinan Seamounts and KPR. For 26 Myr, the sediment piles must be eroded tectonically by subducting ridges which contribute to the delivery of large amount of sediments into the mantle beneath the Chugoku district (Bangs et al., 2006).

6.4. Reactive Infiltration in the Mantle

Because slab melt is silica-saturated, it reacts with peridotite and forms pyroxene-bearing assemblages. This mineralogical reaction is accompanied by chemical mass transfer and geochemical modifications of both the slab melt and the subarc mantle. Below, we address (1) the geochemical modification of the slab melt, (2) the geochemical modification of the subarc mantle, and (3) the transport history of the silica-saturated melt.

6.4.1. Geochemical Modification of Slab Melt and the Genesis of Low-Si and High-Sr Andesite

Trace-element modeling of slab melting does not reproduce the patterns of the Aonoyama and Kurayoshi (aphyric) lavas which show heavy-REE enrichments (Figures 7 and S5). These lavas are also characterized by relatively low SiO_2 (<64 wt %) and high MgO or Mg# (MgO > 2 wt %, Mg# = 55–60; see Figures 6 and 8). This observation is consistent with the geochemistry of the low-Si adakite (Martin et al., 2005) postulated to have formed by interaction with the mantle.

The interaction between siliceous slab melt and mantle is governed by mineralogical reaction described as melt + olivine → orthopyroxene (Kelemen et al., 1993; Yaxley & Green, 1998). In the steady state, melt is frozen in the mantle as pyroxenite. However, Kelemen et al. (1993) emphasized that this interaction occurs under polybaric condition in the wedge mantle with inverted thermal gradient. The combined effect of heating-up and decompression allows melt to infiltrate the mantle without solidification. The effect of melt-mantle interaction on the composition of slab-derived siliceous melts is examined using the assimilation and fractional crystallization model (DePaolo, 1981; Text S1, Figure S6, and Tables S27–28 in the supporting information).

The observed compositions of Aonoyama lavas and Kurayoshi aphyric lavas fit well with a modeled melt with 0.2–0.4% increase of melt volume (F_m = 1.002–1.004, where F_m is mass fraction of reacted melt relative to pristine slab melt). The small F_m obtained in the modeling indicates that the melts in the mantle experienced neither significant peridotite ingestion nor formation of reaction pyroxenite, consistent with their low Mg# (<60). Elements with low C_a/C_m^0 (≪1, where C_a is element concentration of peridotite and C_m^0 is element concentration of pristine melt) are little affected by melt-peridotite interaction (i.e., highly incompatible elements). Accordingly, little modification is anticipated for Sr-, Nd-, and Pb-isotope compositions by peridotite assimilation (C_a^{Sr}/C_m^{Sr0}~0.03, C_a^{Nd}/C_m^{Nd0}~0.1, C_a^{Pb}/C_m^{Pb0}~0.03; Kelemen et al., 2003). Small volume lavas in Aonoyama may indicate the melt transportation by diapirs with smaller radii and slower ascending rate, resulting in relatively higher extent of reaction (higher F_m) among melts formed beneath Chugoku district. Less reactive feature for the other lavas may be attained by production of greater amounts of melt by higher degree of melting, which enables to form larger diapir and ascend faster. In summary, the geochemical features of the low-Si adakitic lavas can be explained by melt-peridotite interaction during their ascent.

6.4.2. Geochemical Modification of Sub-Arc Mantle and the Genesis of Associated Basalts

Basalts occur in close spatial and temporal proximity with the volcanoes of high-Sr andesites and dacites (Figures 3–5). Their magnesian compositions (5–10 MgO wt % Mg# = 50–75; Figures 6 and 8) indicate that they were not significantly affected by shallow-level processes (e.g., fractional crystallization and crustal assimilation). Feineman et al. (2013) observed that the Yokota basalts and Daisen high-Sr andesites and dacites are similarly enriched in Pb, Sr, and Li. We found a similar relationship between the andesites and dacites and associated basalt lavas in the other regions (Figure S4). Trace element patterns of these basalts are characterized by depletion in Nb and Ta (except for two Kurayoshi lavas) and enrichment in Rb, Ba, Th, U, K, Pb, Sr, and Li. Compared with island arc tholeiites, they show marked enrichment in Sr and Th (Figure S7). Kuritani et al. (2008) argued that supercritical fluid from the slab can transport relatively immobile elements such as Th. However, in SW Japan, the slab is at too shallow (depth < 100 km) to form supercritical fluid from the subducting basalt (~180 km; Kessel, Schmidt, et al., 2005). Instead, we suggest that the source of the basalt lavas had previously interacted with slab melt, resulting in change in its composition prior to melting.

We performed trace element forward modeling to examine the interaction between slab melt and wedge mantle (e.g., Yogodzinski et al., 1995). Small amount (1–4 wt %) of slab melt (modeled melts, Figure S5 and Table S25) is mixed with a mantle, then the hybrid source is melted at degree of 1 to 15%. Details about the modeling and the results are shown in Text S2, Figure S8–S23, and Table S27–S33. The modeled melts are compared with the compositions of basaltic lavas from Abu, Mengame, Yokota, and Kurayoshi volcanic fields in Figure 12, showing that the modeled melt compositions fit well with the observed compositions. Two types of lavas are identified; one shows strong negative anomalies of Nb and Ta (low-Nb lava), whereas another shows weak negative anomalies for these elements (high-Nb lava). The high-Nb type occurs in Abu and Kurayoshi, while Mengame and Yokota regions yield the low-Nb type. Trace element patterns of low-Nb lavas are reproduced well by 5% melting of the metasomatized mantle consisting of 96% DMM (depleted MORB mantle) and 4% slab melt in the spinel-stability field. The patterns of high-Nb lavas, however, cannot be reproduced from DMM by applying any f (mass fraction of slab melt to mantle), melting degree, or source mineralogy. Instead, the melting of PUM (primitive upper mantle) source can reproduce the pattern of these high-Nb basalts with f = 4% and degree of melting at 5% in the garnet-stability field, consistent with the melting condition estimated in Kimura et al. (2014) and Kimura (2017).

Several studies have documented the occurrence of high-Nb basalts associated with high-Sr andesites and dacites in the other areas (Bourdon et al., 2002; Sajona et al., 1996). These studies suggest that hydrous phases (amphibole or phlogopite) formed by melt-mantle interaction play a key role in the genesis of this type of basalt. Since these phases can contain high abundance of Nb, the breakdown of them during melting leads to elevated Nb in primary basalt magmas. As these phases also contain abundant potassium, it is expected that basalts are highly potassic, but this is not the case for basalts in Chugoku district. Instead, the results of our trace element modeling indicate that low- and high-Nb magmas are derived by melting of the sources with different extent of melt extraction prior to melt metasomatism under different depths. The Abu and Kurayoshi basalts were formed by melting of more fertile mantle, probably upwelled from deep asthenospheric mantle, under the garnet-stability condition (Figure 13). The Mengame and Yokota basalts were formed by melting of more depleted source at shallower depth (~30 km, Figure 13), which was formed by greater melt extraction during upwelling. Sakuyama et al. (2014) also documented the various extents of

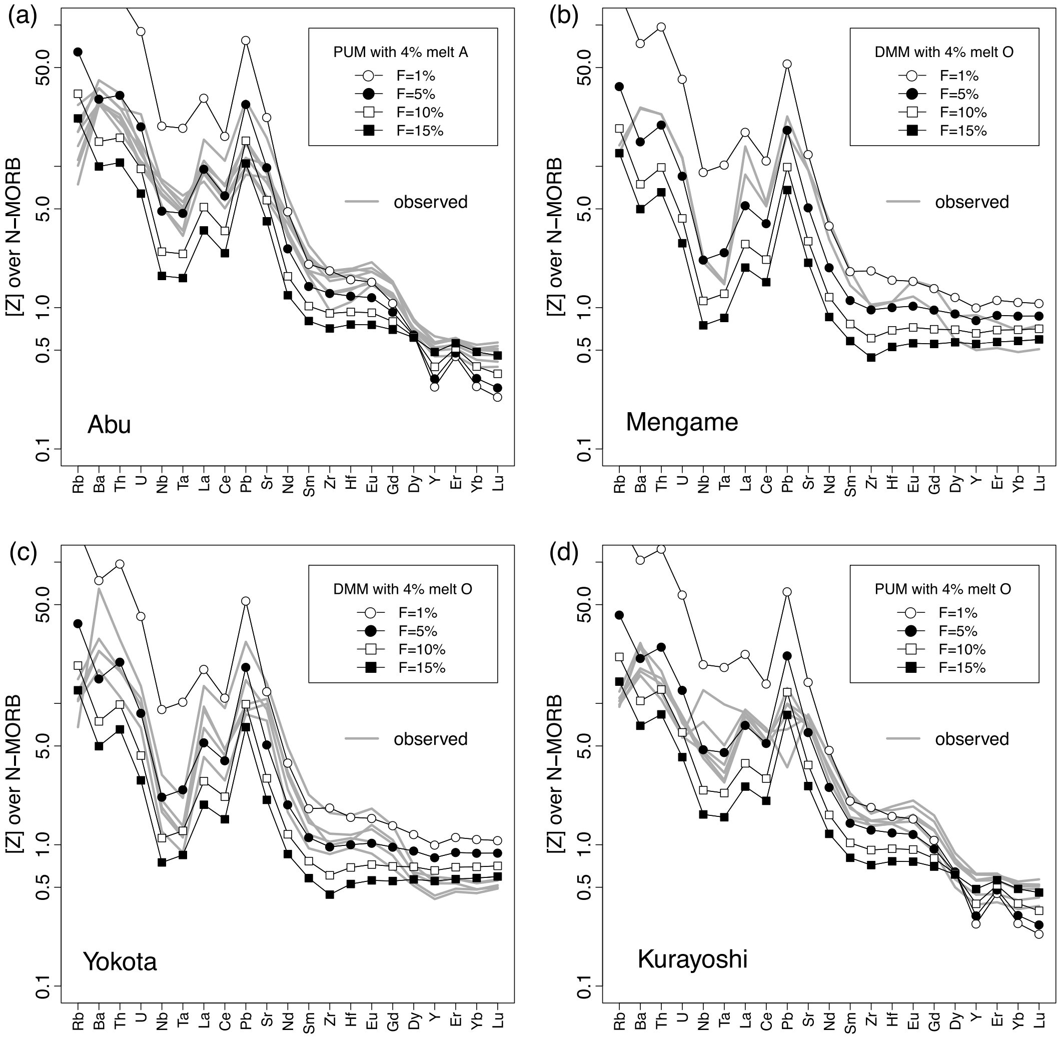

Figure 12. Results of trace element forward modeling for melting of wedge mantle metasomatized by slab melt. Trace element abundances of unmetasomatized wedge mantle are assumed to be either DMM (depleted MORB-source mantle: Workman & Hart, 2005) (Mengame and Yokota) or PUM (McDonough & Sun, 1995; Abu and Kurayoshi). Trace-element compositions of these magma sources are calculated by mixing of DMM or PUM and slab-derived melt at 0.96:0.04 ratio. Primary basalt magma compositions are calculated by a nonmodal batch melting (Shaw, 1970) with varying degree of melting (F = 1–15%) in garnet-stability condition (Abu and Kurayoshi) or spinel-stability condition (Mengame and Yokota). Phase assemblages of the DMM and PUM are taken from Workman and Hart (2005) and McDonough and Rudnick (1998), respectively. Melting mode is taken from Robinson et al. (1998) for spinel-stability condition and from Fram et al. (1998) for garnet-stability condition. Parameters and results of the modeling are summarized in Tables S27–S33. Results of the modeling using the other combination of parameters (source composition and slab-melt fraction) are shown in Figures S8–S23. Trace-element concentration of N-MORB is from Gale et al. (2013). The observed trace element compositions of basalts from Abu, Mengame, Yokota, and Kurayoshi are shown as gray lines on each plot (Tables S6–S9).

Nb enrichment in basalts from northern Kyushu, SW Japan and attributed to polybaric melt extraction from the originally fertile mantle.

6.4.3. Evolution of Magma Conduits

K-Ar ages revealed a temporal relationship between the eruptions of basalt and andesite and dacite magmas (Figures 3–5). In Abu, Wakurayama, Daisen, and Kurayoshi, eruptions of basalt lavas preceded the emplacement of andesites and dacites. Absence of basalt lavas in the upper sequence of andesites and dacites in Sambe and Oe-Takayama also supports the general temporal relationship of the two magma series. The interval of eruptions of the two series is about 1 million years. We discuss the possible causes: (1) the melt transport rate in the mantle and (2) the residence time in shallow-level magma reservoirs. Initial ascent of slab melt may be due to its intrinsic buoyancy. We estimated density of slab melt in the mantle, using major-element compositions and P–T-dependent partial molar volumes of each oxide component (Lange, 1997; Lange & Carmichael, 1987, 1990). In the lowermost wedge mantle close to the slab surface (1,000 °C and 3 GPa),

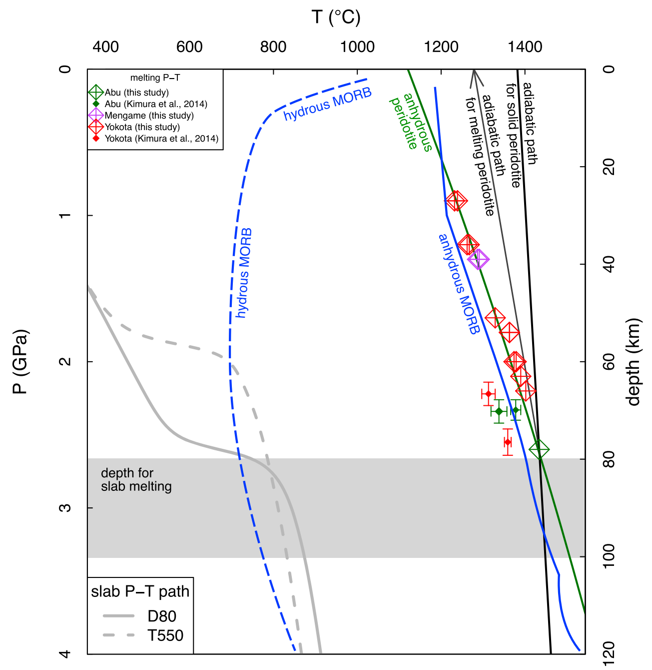

Figure 13. Pressure and temperature (*P–T*) condition of the subducted Shikoku Basin Plate and wedge mantle. The slab *P–T* path is after Syracuse et al. (2010); two models shown are based on partial-to-full viscous coupling between the slab and mantle wedge as functions of depth (D80) or temperature (T550). *P–T* condition of wedge mantle is estimated from major-element compositions of less differentiated basalts from Abu, Mengame, and Yokota (Text S3, Figure S24, and Table S34; Hirose & Kushiro, 1993; Lee & Chin, 2014; Sakuyama et al., 2014; Walker et al., 1979). For comparison, *P–T* estimate by Kimura et al. (2014) are shown (smaller symbol with error bar), which are consistent with our study. Adiabatic paths for solid and melting peridotite are after McKenzie (1984): $dT/dP = 60$ °C · GPa^{-1} for molten peridotite and $dT/dP = 20$ °C · GPa^{-1} for solid peridotite. The mantle potential temperature is estimated to be 1,380 °C. The solidi of peridotite and subducting slab (MORB) are shown for the reference: anhydrous peridotite after Hirschmann (2000), anhydrous MORB after Yasuda et al. (1994), and hydrous MORB after Kessel, Ulmer, et al. (2005).

slab melt has a density ($\rho_{\text{slab melt}}$) of 3,000 to 3,100 kg m^{-3}. A negative density contrast to ambient mantle is 150–300 kg m^{-3} (ρ_{mantle} ~3,250–3,300 kg m^{-3}; Jull & Kelemen, 2001; Figure 14). With its density contrast, slab melt can detach from the subducting slab and be incorporated into overlying mantle (Stolper et al., 1981). Reaction with ambient mantle leads to formation of pyroxenite, which acts as impermeable barrier and facilitates the formation of diapir (Yogodzinski et al., 2015). The viscosity of slab melt ($\rho_{\text{slab melt}}$) estimated from major element compositions (Giordano et al., 2008) is higher (10^5–10^7 Pa · s) than basaltic magmas (Figure 14b), which also facilitates the formation of diaper rather than channelized flow. The percolation velocity (w_0) of mafic melt relative to peridotite is given by McKenzie (1985) as:

$$w_0 = \frac{a^2\phi^3(1-\phi)(\rho_s-\rho_f)g\cdot 10^{-3}}{\mu\phi} \tag{1}$$

where a is grain radius of mantle minerals (10^{-3} m), ϕ is melt fraction (~10%), ρ_s and ρ_f are densities of mantle and melt (3.3×10^3 kg m^{-3} and 2.8×10^3 kg m^{-3}, respectively), g is gravity acceleration (10 m s^{-1}), and μ is shear velocity of melt (1 Pa · s). The w_0 is estimated to be about 1 m yr^{-1}.

The rising velocity of slab melt (w_o') as a mantle diapir is estimated following Marsh (1979) as

$$w_o' = \frac{2}{3}\frac{R^2(\rho_s-\rho_d)g}{\eta_s}\left(\frac{\eta_s+\eta_d}{2\eta_s+3\eta_d}\right) \tag{2}$$

where R is radius of the diapir, ρ_d is density of the diapir (with slab-melt pond), and η_s and η_d are viscosity of solid mantle and diapir, respectively. We assume that ρ_d is 3.1×10^3 kg m^{-3} (Figure 14a), R is 5–10×10^3 m (5–10 km), η_s is 10^{18} Pa · s (Figure 14b), and $\eta_s \gg \eta_d$ (so the factor in bracket becomes 0.5), respectively. The w_o' is estimated to be 0.5–2 m yr^{-1}, indicating identical ascent rates for the mantle-derived basalt and slab-derived siliceous melts.

We therefore suggest that the apparent gap in time between the eruption of basalt and the eruption of high-Sr andesite and dacite (~1 Myr) can be attributed to shallow-level crustal processes, rather than melt transport processes in the mantle. Short residence time is inferred for basalt magmas based on their less differentiated features. Hence, the gap in time of eruptions relies essentially on residence time of high-Sr andesite and dacite magmas in the intracrustal reservoir. Numerical studies support the residence time of 1 million years for large-volume reservoir filled by intermediate-felsic magma (Kaiser et al., 2017; Karakas et al., 2017).

6.5. Evolution of Shikoku Basin Plate

During subduction, the sediment, oceanic crust, and uppermost mantle of the subducting plate undergo progressive metamorphism accompanied with dehydration reactions (Poli & Schmidt, 2002). The depth of dehydration reactions varies with temperature of the subducting slabs (Peacock, 2009). The Shikoku Basin Plate is young and hot, and therefore, the crustal section dehydrates at shallow depth (50–80 km) with transformation to eclogite-facies rocks (Kimura, 2017; Kimura et al., 2014; Peacock & Wang, 1999). In the greater depth, the fluids are released mainly from serpentinite in the mantle section of the subducting slab (Kimura et al., 2014; Poli & Schmidt, 2002; Portnyagin et al., 2007; Ringwood, 2013; Walowski et al., 2015).

Melting temperatures for subducting slabs are largely affected by the presence of water. Experimental studies have demonstrated that solidus temperatures of dry and wet basaltic rocks differ by 500–700 °C at depths for slab melting (Kessel, Ulmer, et al., 2005; Yasuda et al., 1994). The temperature of subducted Shikoku Basin Plate, predicted by a numerical model (Syracuse et al., 2010), intersects wet basalt solidus at

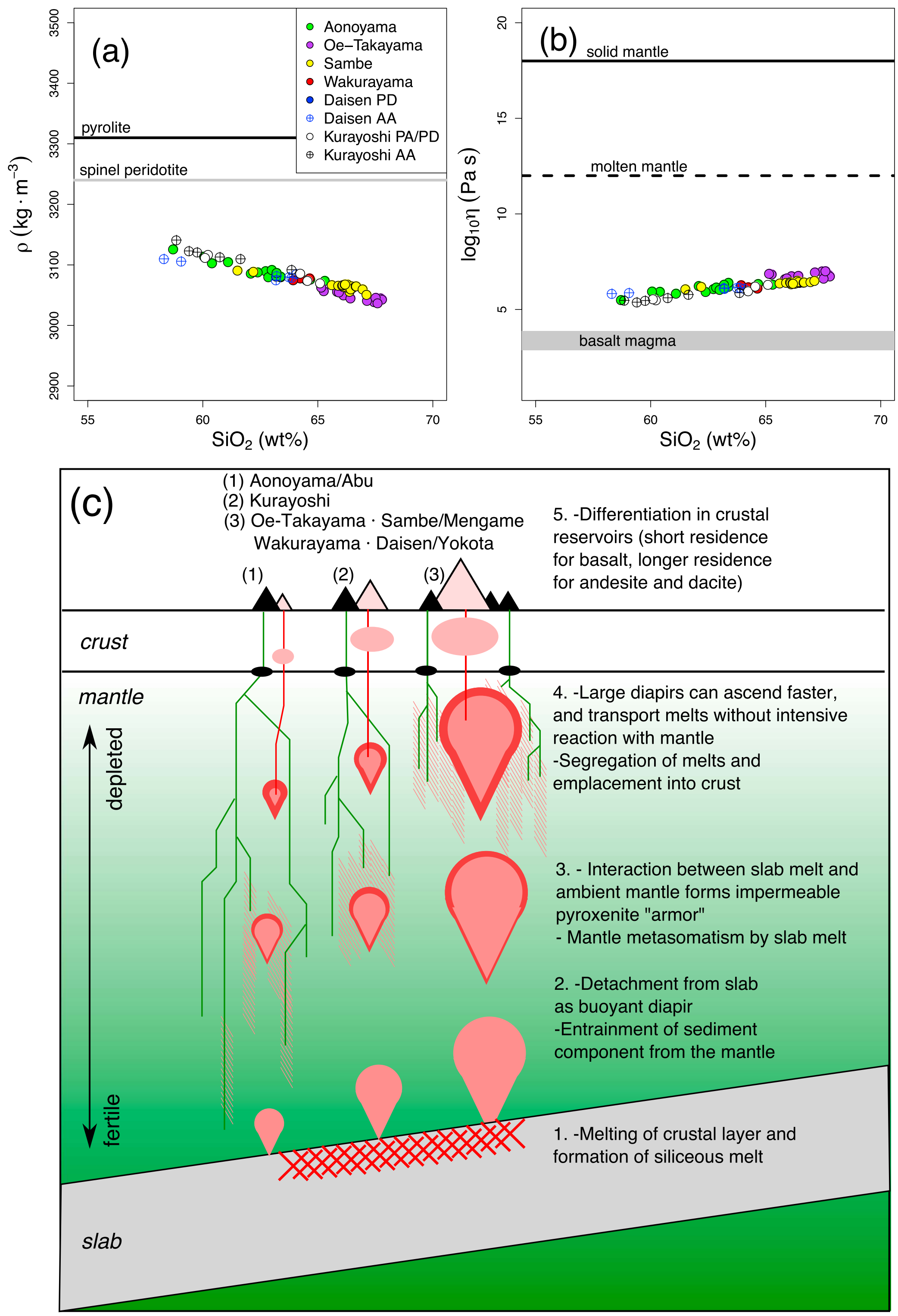

Figure 14. Physical properties of slab melts in the wedge mantle (80–100 km depth) and the implication for the evolution of melt conduits. (a) A negative density contrast of slab melt to the overlying mantle is 150–300 kg · m^{-3} (black line, pyrolite; gray line, spinel peridotite; Jull & Kelemen, 2001). (b) Viscosity contrast of slab melt to the overlying mantle (solid line, solid state; broken line, molten state; Jin et al., 1994; Stevenson, 1994) and basalt magmas (gray bar, estimated using major-element compositions in Table S34). (c) A schematic cartoon of conduits of slab melt and basalt magma. Basalt magmas would have been transported by channelized flow. Slab melts would have been transported as diapirs.

10.1029/2017JB015066

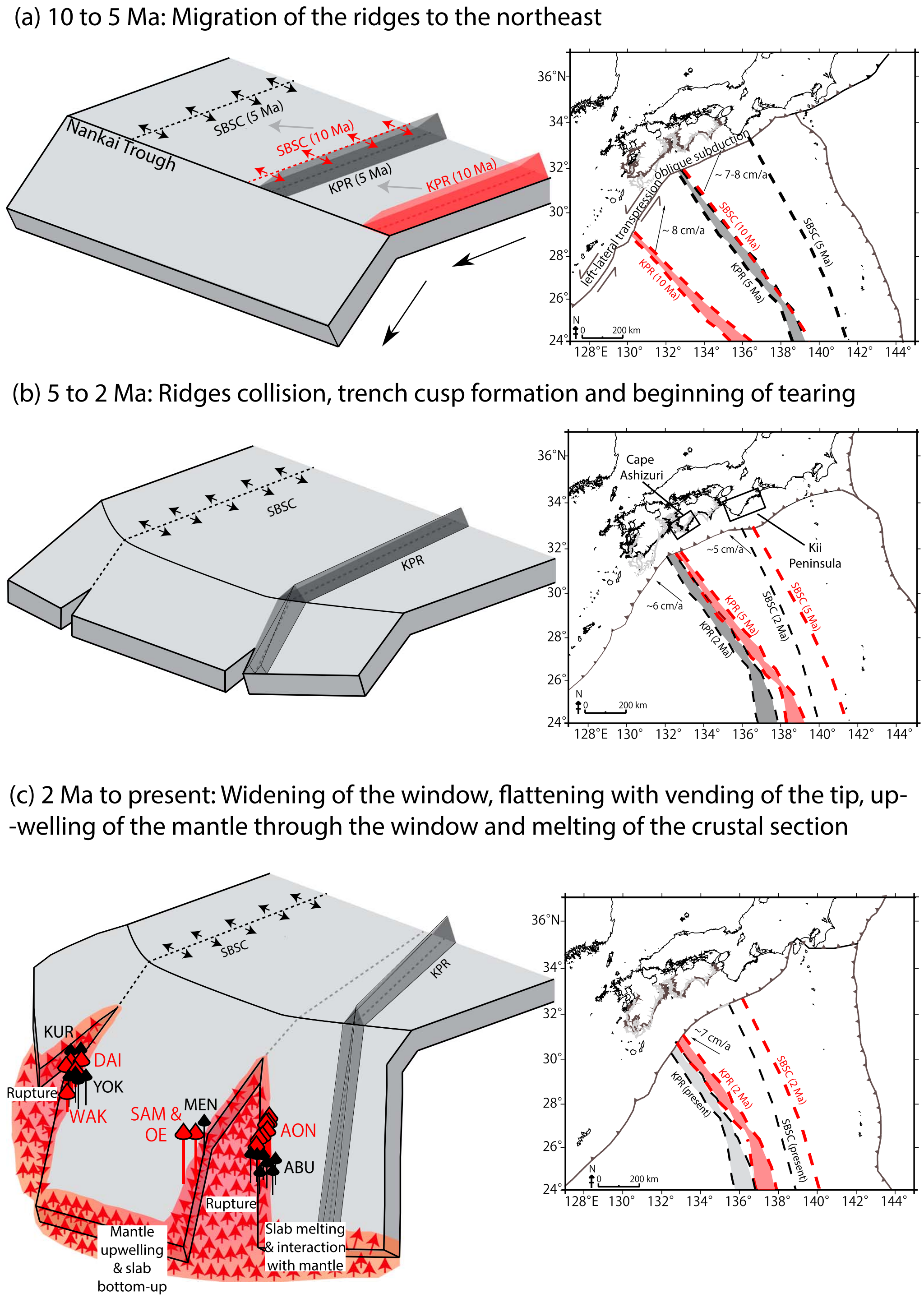

Figure 15. A schematic illustration for the evolution of Shikoku Basin Plate, in comparison with paleotectonic reconstruction (inset maps) of Mahony et al. (2011). (a) 10–5 Ma: The Kyushu-Palau Ridge (KPR) and Shikoku Basin Spreading Center (SBSC) had migrated from south to north. (b) 5–2 Ma: At around 5 Ma, the KPR was located in the south of Cape Ashizuri, whereas the SBSC was located in the south of Kii Peninsula. In the ensuing period, these ridges collided with the Nankai Trough and resulted in the arcuate trench. Subduction into the trench caused lateral tension on the slab and began to tear apart. (c) 2 Ma to present: Tearing of slab was propagated, presumably to due flattening of slab by mantle bottoming up. At the tears, hot and buoyant mantle had upwelled adiabatically and caused dehydration of the mantle section and melting of the crustal section in the subducting slab. The mantle was metasomatized by slab melt and melted to produce the basalts erupted close to high-Sr andesites and dacites. Siliceous slab melt could infiltrate without solidification by heat supplied from the mantle and decompression during ascent.

60–80 km, indicating the likelihood of slab melting if it is hydrated (Figure 13). The occurrence of hornblende in high-Sr andesites and dacites (Figure S1) is consistent with melt production under hydrous condition (2 wt % or more water in melts; Green, 1972).

Geochemical studies of basalts suggest that the wedge mantle beneath the Chugoku district is less hydrous compared to the mantle beneath NE Japan (Kimura et al., 2014; Kimura, 2017; Zellmer et al., 2012, 2014, 2015). This may suggest that dehydration of serpentinite does not occur on the widespread regions of the slab, and rather confined to melting regions of the slab. Seismic tomography showed that the volcanoes of high-Sr andesites and dacites are located above aseismic slab discontinuity and low-velocity anomaly in the subslab mantle (Asamori & Zhao, 2015; Nakajima & Hasegawa, 2007; Zhao et al., 2018). This observation suggests that slab melting occurred at tears of the subducting slab as a result of interaction with a hot and buoyant mantle (e.g., Yogodzinski et al., 2001).

The *P*–*T* condition of wedge mantle is estimated from major-element composition of less differentiated basalts. Details of the method are given in Text S3. The estimated *P*–*T* are shown in Figure 13 (also summarized in Table S34), which are essentially consistent with the previous studies (Kimura et al., 2014; Tamura et al., 2000). Variation in the obtained *P*–*T* conditions indicates that a hot and buoyant mantle (~1,400 °C at 80 km) upwelled from the depth corresponding to that for slab melting inferred from the aseismic slab contours (Zhao et al., 2012, 2018). We therefore conclude that a hot and buoyant mantle could assist intensive dehydration in the mantle section and melting of the overlying crustal section of the subducting slab at its tears.

We speculated that the cause of tearing on the slab is subduction of oceanic ridges. Two prominent ridges are observed on the Shikoku Basin Plate (Figure 1): KPR and SBSC. The formation ages for these ridges are dated to be 28–25 Ma for KPR (Ishizuka et al., 2011) and 15–11 Ma for SBSC (Ishizuka et al., 2009), and the ridges are subducting at a rate of 22.4 km Myr^{-1} estimated from convergent velocity (43 km Myr^{-1}) and slab dip (31.4°; see Syracuse et al., 2010). At that rate, the slab beneath the volcanoes of high-Sr andesites and dacites (80–100 km depth) had initially subducted into the trench at 5–4 Ma. A plate reconstruction model shows that, at 5 Ma, the KPR and SBSC were located at the extension of the slab tears along the plate convergence vector (Figure 1; see Mahony et al., 2011), providing convincing evidence for the causal link between slab tearing and ridge subduction.

We here provide a conceptual model for the formation of slab tear and production of high-Sr andesite and dacite magmas (see the illustration in Figure 15). The KPR and SBSC had formed by subduction of the Pacific Plate beneath the Philippine Sea Plate and migrated to the northeast during the period of 10–5 Ma (Figure 15a; Mahony et al., 2011). Around 5 Ma, the plate kinematics of the Philippine Sea plate changed, and KPR and SBSC had been located in the south of Cape Ashizuri and Kii Peninsula, respectively (Figure 15b). The collision of the KPR and SBSC could have formed the arcuate trench at the Nankai Trough (Mason et al., 2010). Subsequent subduction resulted in lateral tension on the slab, which eventually was torn apart at the leading edge (Figure 15b; Cao et al., 2014). With time, the subduction angle would shallow due to dynamic support from a hot and buoyant mantle. This may also facilitate propagation of the slab tear. Since 2 Ma, the interaction of the mantle and slab has been enhanced, presumably related to widening of the slab tear (Figure 15c). The vigorous upwelling of hot and buoyant mantle could have allowed silica-saturated slab melt to infiltrate without solidification, leading to the production of basaltic volcanoes adjacent to the eruptions of high-Sr andesite and dacites.

7. Conclusions

Geochronological analyses of late Cenozoic volcanic rocks from the SW Japan arc revealed that the eruptions of high-Sr andesite and dacite lavas began at 2 Ma and continued to the recent. Five volcanic fields are recognized as the loci of high-Sr andesite and dacite volcanism in the Chugoku district. In all of these regions, basalts occur in close spatial and temporal proximity to high-Sr andesites and dacites.

Geochemistry of the high-Sr andesite and dacite is best explained by melting of the subducted oceanic crust of Shikoku Basin Plate with a component of melted sediment. Significant contributions of sediments are found in all volcanic fields in central Chugoku. This could be due to sediment accumulation within the trench and subduction erosion by the ridges on Shikoku Basin Plate.

Spatial and temporal coincidence of basalt and high-Sr andesite and dacite suggests the co-genetic relationship. The most likely explanation is that the slab had interacted with mantle. Major and trace element compositions of high-Sr andesites and dacites and basalts provide evidence for their thermochemical interaction. Low-Si and high-Sr andesites in Aonoyama and Kurayoshi had been produced by greater extent of peridotite assimilation. Melting of mantle reacted with slab melt could also yield Sr-, Ba-, and Pb-enriched magmas, as observed in associated basalt lavas.

The spatial coincidence of the high-Sr andesite and dacite volcanoes and the seismic gap in the subducting slab suggests that slab melting occurred at its tears. A hot and buoyant mantle could have upwelled through the tears from subslab depths, bolstering dehydration of the mantle section and melting of the crustal section in the subducting slab. Adiabatic decompression driven by upwelling mantle prevents the “freezing” of siliceous slab melt as pyroxenite in the mantle.

Acknowledgments
We are grateful to G. E. Bebout for discussion and improving the manuscript. We would also like to thank S. Tokeshi and T. Yemer for help in the sampling and geochemical analysis of granitic rocks in Chugoku district. All members of Pheasant Memorial Laboratory are thanked for their technical support, constructive discussion, and encouragement. Gene Yogodzinski and an anonymous reviewer are thanked for their helpful review, and Michael Walter for his editorial handling. All the data used for this study are included in the supporting information. This study was supported by the MEXT (Ministry of Education, Culture, Sports, Science and Technology). Maps (Figures 1, 3, 4 and 5) were created using the Generic Mapping Tools (Wessel et al., 2013).

References

Alonso-Perez, R., Müntener, O., & Ulmer, P. (2009). Igneous garnet and amphibole fractionation in the roots of island arcs: Experimental constraints on andesitic liquids. *Contributions to Mineralogy and Petrology*, *157*(4), 541–558.

Arndt, N. T., & Goldstein, S. L. (1989). An open boundary between lower continental crust and mantle: Its role in crust formation and crustal recycling. *Tectonophysics*, *161*(3), 201–212.

Asamori, K., & Zhao, D. (2015). Teleseismic shear wave tomography of the Japan subduction zone. *Geophysical Journal International*, *203*(3), 1752–1772.

Atherton, M. P., & Petford, N. (1993). Generation of sodium-rich magmas from newly underplated basaltic crust. *Nature*, *362*(6416), 144–146. https://doi.org/10.1038/362144a0

Baksi, A. K., Archibald, D. A., & Farrar, E. (1996). Intercalibration of $^{40}Ar/^{39}Ar$ dating standards. *Chemical Geology*, *129*(3), 307–324.

Ban, M., & Yamamoto, T. (2002). Petrological study of Nasu-Chausudake volcano (ca. 16 ka to present), northeastern Japan. *Bulletin of Volcanology*, *64*(2), 100–116.

Bangs, N. L. B., Gulick, S. P. S., & Shipley, T. H. (2006). Seamount subduction erosion in the Nankai Trough and its potential impact on the seismogenic zone. *Geology*, *34*(8), 701–704.

Bourdon, E., Eissen, J.-P., Monzier, M., Robin, C., Martin, H., Cotten, J., & Hall, M. L. (2002). Adakite-like lavas from Antisana volcano (Ecuador): Evidence for slab melt metasomatism beneath Andean Northern Volcanic Zone. *Journal of Petrology*, *43*(2), 199–217.

Boynton, W. V. (1983). Cosmochemistry of the rare earth elements: Meteorite studies. In P. Henderson (Ed.), *Rare earth element geochemistry* (pp. 63–114). New York: Elsevier.

Cao, L., Wang, Z., Wu, S., & Gao, X. (2014). A new model of slab tear of the subducting Philippine Sea Plate associated with Kyushu-Palau Ridge subduction. *Tectonophysics*, *636*, 158–169.

Castillo, P. R., Floyd, P. A., & France-Lanord, C. (1992). Isotope geochemistry of Leg 129 basalt: Implications for the origin of the widespread Cretaceous volcanic event in the Pacific. *Proceedings of the Ocean Drilling Program*, *129*, 405–413. https://doi.org/10.2973/odp.proc.sr.129.131.1992

Defant, M. J., & Drummond, M. S. (1990). Derivation of some modern arc magmas by melting of young subducted lithosphere. *Nature*, *347*(6294), 662–665.

Defant, M. J., & Kepezhinskas, P. (2001). Evidence suggests slab melting in arc magmas. *Eos, Transactions American Geophysical Union*, *82*(6), 65–69.

DePaolo, D. J. (1981). Trace element and isotopic effects of combined wallrock assimilation and fractional crystallization. *Earth and Planetary Science Letters*, *53*(2), 189–202.

Domitsu, H., Shiihara, M., Torii, M., Tsukawaki, S., & Oda, M. (2002). Tephrostratigraphy of the piston cored sediment KT96-17 P-2 in the southern Japan Sea: The eruption age of Daisen-Kusadanihara Pumice (KsP). *Journal of Geological Society of Japan*, *108*(9), 545–556.

Feineman, M., Moriguti, T., Yokoyama, T., Terui, S., & Nakamura, E. (2013). Sediment enriched adakitic magmas from the Daisen volcanic field, southwest Japan. *Geochemistry, Geophysics, Geosystems*, *14*, 3009–3031. https://doi.org/10.1002/ggge.20176

Feyissa, D. H., Shinjo, R., Kitagawa, H., Meshesha, D., & Nakamura, E. (2017). Petrologic and geochemical characterization of rift-related magmatism at the northernmost Main Ethiopian Rift: Implications for plume-lithosphere interaction and the evolution of rift mantle sources. *Lithos*, *282*, 240–261.

Fram, M. S., Lesher, C. E., & Volpe, A. M. (1998). Mantle melting systematics: Transition from continental to oceanic volcanism on the Southeast Greenland margin. In *Proceedings of the Ocean Drilling Program*, *Scientific Results* (Vol. 152, pp. 373–383). TX: Ocean Drilling Program.

Fujinawa, A. (1988). Tholeiitic and calc-alkaline magma series at Adatara volcano, Northeast Japan: 1. Geochemical constraints on their origin. *Lithos*, *22*(2), 135–158.

Fujinawa, A. (1992). Distinctive REE patterns for tholeiitic and calc-alkaline magma series co-occurring at Adatara volcano, Northeast Japan. *Geochemical Journal*, *26*(6), 395–409. https://doi.org/10.2343/geochemj.26.395

Furuyama, K., Nagao, K., & Murata, M. (2002). K-Ar ages of andesites from two volcanic arrays in western Chugoku, southwest Japan. *Volcano (Kazan)*, *47*(5), 481–487.

Gaffney, A. M., Nelson, B. K., & Blichert-Toft, J. (2005). Melting in the Hawaiian plume at 1–2 Ma as recorded at Maui Nui: The role of eclogite, peridotite, and source mixing. *Geochemistry, Geophysics, Geosystems*, *6*, Q10L11. https://doi.org/10.1029/2005GC000927

Gale, A., Dalton, C. A., Langmuir, C. H., Su, Y., & Schilling, J.-G. (2013). The mean composition of ocean ridge basalts. *Geochemistry, Geophysics, Geosystems*, *14*, 489–518. https://doi.org/10.1029/2012GC004334

Gao, S., Rudnick, R. L., Yuan, H.-L., Liu, X.-M., Liu, Y.-S., Xu, W.-L., et al. (2004). Recycling lower continental crust in the North China Craton. *Nature*, *432*(7019), 892–897.

Giordano, D., Russell, J. K., & Dingwell, D. B. (2008). Viscosity of magmatic liquids: A model. *Earth and Planetary Science Letters*, *271*(1), 123–134.

Green, T. H. (1972). Crystallization of calc-alkaline andesite under controlled high-pressure hydrous condition. *Contributions to Mineralogy and Petrology*, *34*(2), 150–166.

Grove, T. L., Kinzler, R. J., Baker, M. B., Donnelly-Nolan, J. M., & Lesher, C. E. (1988). Assimilation of granite by basaltic magma at burnt lava flow, Medicine Lake volcano, northern California: Decoupling of heat and mass transfer. *Contributions to Mineralogy and Petrology*, *99*(3), 320–343. https://doi.org/10.1007/BF00375365

Hart, S. R. (1984). A large-scale isotope anomaly in the southern hemisphere mantle. *Nature*, *309*, 753–757. https://doi.org/10.1038/309753a0

Hattori, H., Kano, K., Suzuki, T., Yokoyama, S., Matsuura, H., & Satoh, H. (1983). Geology of the Sambesan district (Tech. Rep.). Geological Survey of Japan.

Hattori, H., & Katada, M. (1964). Geology of the Neu district (Tech. Rep.). Geological Survey of Japan.

Hauff, F. K., Hoernle, K., & Schmidt, A. (2003). Sr-Nd-Pb composition of Mesozoic Pacific oceanic crust (Site 1149 and 801, ODP Leg 185): Implications for alteration of oceanic crust and the input into the Izu-Bonin-Mariana subduction system. *Geochemistry, Geophysics, Geosystems*, *4*(8), 8913. https://doi.org/10.1029/2002GC000421

Hickey-Vargas, R. (1991). Isotope characteristics of submarine lavas from the Philippine Sea: Implications for the origin of arc and basin magmas of the Philippine tectonic plate. *Earth and Planetary Science Letters*, *107*(2), 290–304.

Hickey-Vargas, R. (1998). Origin of the Indian Ocean-type isotopic signature in basalts from Philippine Sea Plate spreading centers: An assessment of local versus large-scale processes. *Journal of Geophysical Research*, *103*(B9), 209,603–220,979. https://doi.org/10.1029/98JB0252

Hirose, K., & Kushiro, I. (1993). Partial melting of dry peridotites at high pressures: Determination of compositions of melts segregated from peridotite using aggregates of diamond. *Earth and Planetary Science Letters*, *114*(4), 477–489.

Hirschmann, M. M. (2000). Mantle solidus: Experimental constraints and the effects of peridotite composition. *Geochemistry, Geophysics, Geosystems*, *1*(10), 1042. https://doi.org/10.1029/2000GC000070

Hunter, A. G., & Blake, S. (1995). Petrogenetic evolution of a transitional tholeiitic-calc alkaline series: Towada volcano, Japan. *Journal of Petrology*, *36*(6), 1579–1605.

Ike, T., Moore, G. F., Kuramoto, S., Park, J.-O., Kaneda, Y., & Taira, A. (2008). Variations in sediment thickness and type along the northern Philippine Sea Plate at the Nankai Trough. *Island Arc*, *17*(3), 342–357.

Ishiga, H., Suzuki, M., Iizumi, S., Nishimura, K., Kagami, H., & Tanaka, S. (1989). Western extension of Hida terrane: With special reference to gneisses and mylonites discovered in Mizoguchi-cho, western part of Daisen, Tottori Prefecture, southwest Japan. *Journal of Geological Society of Japan*, *95*(2), 129–132.

Ishikawa, T., & Nakamura, E. (1994). Origin of the slab component in arc lavas from across-arc variation of B and Pb isotopes. *Nature*, *370*(6486), 205–208. https://doi.org/10.1038/370205a0

Ishizuka, O., Taylor, R. N., Yuasa, M., & Ohara, Y. (2011). Making and breaking an island arc: A new perspective from the Oligocene Kyushu-Palau arc, Philippine Sea. *Geochemistry, Geophysics, Geosystems*, *12*, Q05005. https://doi.org/10.1029/2010GC003440

Ishizuka, O., Yuasa, M., Taylor, R. N., & Sakamoto, I. (2009). Two contrasting magmatic types coexist after the cessation of back-arc spreading. *Chemical Geology*, *266*(3), 274–296.

Itoh, J. (1990). Petrology of Himeshima volcanic group. *Journal of Mineralogy Petrology and Economic Geology*, *85*(12), 541–558.

Iwamori, H. (1991). Zonal structure of Cenozoic basalts related to mantle upwelling in southwest Japan. *Journal of Geophysical Research*, *96*(B4), 6157–6170. https://doi.org/10.1029/90JB02399

Iwaya, T., & Kurasawa, H. (1986). Petrography and chemistry of Himeshima volcanic rocks in Oita, southwest Japan. *The Journal of the Japanese Association of Mineralogists, Petrologists and Economic Geologists*, *81*(8), 291–301.

Janney, P. E., & Castillo, P. R. (1997). Geochemistry of Mesozoic Pacific mid-ocean ridge basalt: Constraints on melt generation and the evolution of the Pacific upper mantle. *Journal of Geophysical Research*, *102*(B3), 5207–5229. https://doi.org/10.1029/96JB03810

Jin, Z.-M., Green, H. W., & Zhou, Y. (1994). Melt topology in partially molten mantle peridotite during ductile deformation. *Nature*, *372*(6502), 164–167.

Johnson, M. C., & Plank, T. (1999). Dehydration and melting experiments constrain the fate of subducted sediments. *Geochemistry, Geophysics, Geosystems*, *1*(12), 1007. https://doi.org/10.1029/1999GC000014

Jull, M., & Kelemen, P. B. (2001). On the conditions for lower crustal convective instability. *Journal of Geophysical Research*, *106*(B4), 6423–6446. https://doi.org/10.1029/2000JB900357

Kaiser, J. F., de Silva, S., Schmitt, A. K., Economos, R., & Sunagua, M. (2017). Million-year melt-presence in monotonous intermediate magma for a volcanic-plutonic assemblage in the Central Andes: Contrasting histories of crystal-rich and crystal-poor super-sized silicic magmas. *Earth and Planetary Science Letters*, *457*, 73–86.

Kakubuchi, S., Nagao, T., & Nagao, K. (2000). K-Ar ages and magmatic history of the Abu Monogenetic Volcano Group, southwest Japan. *Japanese Magazine of Mineralogical and Petrological Sciences*, *29*, 191–198.

Kamata, H. (1989). Volcanic and structural history of the Hohi volcanic zone, central Kyushu, Japan. *Bulletin of Volcanology*, *51*(5), 315–332.

Kamata, H., Hoshizumi, H., & Koyaguchi, T. (1987). The formation age of the volcanic front in central Kyushu-western Chugoku district. In *Programme and abstracts the volcanological society of Japan* (chap. 31, 85 pp.). Tokyo: Volcanological Society of Japan.

Kaneoka, I., & Suzuki, M. (1970). K-Ar and fission track ages of some obsidian from Japan. *Journal of the Geological Society of Japan*, *76*(6), 309–313. https://doi.org/10.5575/geosoc.76.309

Kano, K., Takarada, S., Makimoto, H., Tsuchiya, N., & Bunno, M. (2000). Geology of the Yunotsu and Gotsu districts (Tech. Rep.). Geological Survey of Japan.

Kano, K., Yamaguchi, S., Takayasu, K., Matsuura, H., & Bunno, M. (1994). Geology of the Matsue district (Tech. Rep.). Geological Survey of Japan.

Karakas, O., Degruyter, W., Bachmann, O., & Dufek, J. (2017). Lifetime and size of shallow magma bodies controlled by crustal-scale magmatism. *Nature Geoscience*, *10*(6), 446–450.

Katsumata, A. (2010). Depth of the Moho discontinuity beneath the Japanese Islands estimated by traveltime analysis. *Journal of Geophysical Research*, *115*, B04303. https://doi.org/10.1029/2008JB005864

Kawai, N., & Hirooka, K. (1967). Results of dating on Cenozoic igneous rocks from southwest Japan. *Journal of Geological Society of Japan*, *73*(2), 68.

Kay, R. W. (1978). Aleutian magnesian andesites: Melts from subducted Pacific Ocean crust. *Journal of Volcanology and Geothermal Research*, *4*(1-2), 117–132. https://doi.org/10.1016/0377-0273(78)90032-X

Kelemen, P. B., Hart, S. R., & Bernstein, S. (1998). Silica enrichment in the continental upper mantle via melt/rock reaction. *Earth and Planetary Science Letters*, *164*(1), 387–406.

Kelemen, P. B., Shimizu, N., & Dunn, T. (1993). Relative depletion of niobium in some arc magmas and the continental crust: Partitioning of K, Nb, La and Ce during melt/rock reaction in the upper mantle. *Earth and Planetary Science Letters*, *120*(3), 111–134.

Kelemen, P. B., Yogodzinski, G. M., & Scholl, D. W. (2003). Along-strike variation in the Aleutian Island Arc: Genesis of high Mg# andesite and implications for continental crust. In J. Eiler (Ed.), *Inside the subduction factory*, *Geophysical Monograph Series* (Vol. 138, pp. 223–276). Washington, DC: American Geophysical Union.

Kepezhinskas, P., Defant, M. J., & Drummond, M. S. (1996). Progressive enrichment of island arc mantle by melt-peridotite interaction inferred from Kamchatka xenoliths. *Geochimica et Cosmochimica Acta*, *60*(7), 1217–1229. https://doi.org/10.1016/0016-7037(96)00001-4

Kessel, R., Schmidt, M. W., Ulmer, P., & Pettke, T. (2005). Trace element signature of subduction-zone fluids, melts and supercritical liquids at 120–180 km depth. *Nature*, *437*(7059), 724–727.

Kessel, R., Ulmer, P., Pettke, T., Schmidt, M. W., & Thompson, A. B. (2005). The water-basalt system at 4 to 6 GPa: Phase relations and second critical endpoint in a K-free eclogite at 700 to 1400 °C. *Earth and Planetary Science Letters*, *237*(3), 873–892.

Kimura, J.-I. (2017). Modeling chemical geodynamics of subduction zones using the arc basalt simulator version 5. *Geosphere*, *13*(4), 992–1025.

Kimura, J.-I., Gill, J. B., Kunikiyo, T., Osaka, I., Shimoshioiri, Y., Katakuse, M., et al. (2014). Diverse magmatic effects of subducting a hot slab in SW Japan: Results from forward modeling. *Geochemistry, Geophysics, Geosystems*, *15*, 691–739. https://doi.org/10.1002/2013GC005132

Kimura, J.-I., Kunikiyo, T., Osaka, I., Nagao, T., Yamauchi, S., Kakubuchi, S., et al. (2003). Late Cenozoic volcanic activity in the Chugoku area, southwest Japan arc during back-arc basin opening and reinitiation of subduction. *Island Arc*, *12*(1), 22–45.

Kimura, J.-I., Miyazaki, T., Vaglarov, B. S., Haraguchi, S., Chang, Q., & Gill, J. B. (2015). Reply to comment by I. Pineda-Velasco, T T Nguyen, H. Kitagawa, and E. Nakamura on "Diverse magmatic effects of subducting a hot slab in SW Japan: Results from forward modeling". *Geochemistry, Geophysics, Geosystems*, *16*, 2853–2857. https://doi.org/10.1002/2015GC005984

Kimura, J.-I., Stern, R. J., & Yoshida, T. (2005). Reinitiation of subduction and magmatic responses in SW Japan during Neogene time. *Geological Society of America Bulletin*, *117*(7), 969–986. https://doi.org/10.1130/B25565.1

Kimura, J.-I., & Yoshida, T. (2006). Contributions of slab fluid, mantle wedge and crust to the origin of quaternary lavas in the NE Japan arc. *Journal of Petrology*, *47*(11), 2185–2232. https://doi.org/10.1093/petrology/egl041

Kimura, J.-I., Yoshida, T., & Iizumi, S. (2002). Origin of low-K intermediate lavas at Nekoma volcano, NE Honshu Arc, Japan: Geochemical constraints for lower-crustal melts. *Journal of Petrology*, *43*(4), 631–661.

Klimm, K., Blundy, J. D., & Green, T. H. (2008). Trace element partitioning and accessory phase saturation during H_2O-saturated melting of basalt with implications for subduction zone chemical fluxes. *Journal of Petrology*, *49*(3), 523–553. https://doi.org/10.1093/petrology/egn001

Koyaguchi, T. (1986). Textural and compositional evidence for magma mixing and its mechanism, Abu volcano group, southwestern Japan. *Contributions to Mineralogy and Petrology*, *93*(1), 33–45.

Kudo, T., Sasaki, M., Uchiyama, Y., Nozawa, A., Sasaki, H., Tokizawa, T., & Takarada, S. (2007). Petrological variation of large-volume felsic magmas from Hakkoda-Towada caldera cluster: Implications for the origin of high-k felsic magmas in the Northeast Japan Arc. *Island Arc*, *16*(1), 133–155.

Kumura, K., Kanaori, Y., & Toshida, K. (2002). K-Ar ages of Aonoyama monogenetic volcanoes and implications for the tectonic evolution of Tokusa and Tsuwano basins, Programme and abstracts the Geological Society of Japan, 109, 286.

Kuno, H. (1966). Lateral variation of basalt magma type across continental margins and island arcs. *Bulletin Volcanologique*, *29*(1), 195–222. https://doi.org/10.1007/BF02597153

Kuritani, T., & Nakamura, E. (2002). Precise isotope analysis of nanogram-level Pb for natural rock samples without use of double spikes. *Chemical Geology*, *186*(1), 31–43.

Kuritani, T., & Nakamura, E. (2003). Highly precise and accurate isotopic analysis of small amounts of Pb using ^{205}Pb-^{204}Pb and ^{207}Pb-^{204}Pb, two double spikes. *Journal of Analytical Atomic Spectrometry*, *18*(12), 1464–1470.

Kuritani, T., Yokoyama, T., & Nakamura, E. (2008). Generation of rear-arc magmas induced by influx of slab-derived supercritical liquids: Implications from alkali basalt lavas from Rishiri volcano, Kurile arc. *Journal of Petrology*, *49*(7), 1319–1342. https://doi.org/10.1093/petrology/egn027

Kuritani, T., Yoshida, T., Kimura, J.-I., Hirahara, Y., & Takahashi, T. (2014). Water content of primitive low-k tholeiitic basalt magma from Iwate volcano, NE Japan Arc: Implications for differentiation mechanism of frontal-arc basalt magmas. *Mineralogy and Petrology*, *108*(1), 1–11.

Kuritani, T., Yoshida, T., Kimura, J.-I., Takahashi, T., Hirahara, Y., Miyazaki, T., et al. (2014). Primary melt from Sannome-Gata Volcano, NE Japan Arc: Constraints on generation conditions of rear-arc magmas. *Contributions to Mineralogy and Petrology*, *167*(2), 969. https://doi.org/10.1007/s00410-014-0969-7

Lange, R. A. (1997). A revised model for the density and thermal expansivity of K_2O-Na_2O-CaO-MgO-Al_2O_3-SiO_2 liquids from 700 to 1900 K: Extension to crustal magmatic temperatures. *Contributions to Mineralogy and Petrology*, *130*(1), 1–11.

Lange, R. A., & Carmichael, I. S. E. (1987). Densities of Na_2O-K_2O-CaO-MgO-FeOFe$_2O_3$-Al_2O_3-TiO_2-SiO_2 liquids: New measurements and derived partial molar properties. *Geochimica et Cosmochimica Acta*, *51*(11), 2931–2946. https://doi.org/10.1016/0016-7037(87)90368-1

Lange, R. A., & Carmichael, I. S. E. (1990). Thermodynamic properties of silicate liquids with emphasis on density, thermal expansion and compressibility. *Reviews in Mineralogy and Geochemistry*, *24*(1), 25–64.

Langmuir, C. H., Vocke, R. D., Hanson, G. N., & Hart, S. R. (1978). A general mixing equation with applications to Icelandic basalts. *Earth and Planetary Science Letters*, *37*(3), 380–392.

Le Maitre, R. W., Bateman, P., Dudek, A., Keller, J., Lameyre, J., Le Bas, M. J., et al. (1989). *A classification of igneous rocks and glossary of terms: Recommendations of the International Union of Geological Sciences Subcommission on the Systematics of Igneous Rocks* (193 pp.). Oxford: Blackwell.

Lee, C.-T. A., & Chin, E. J. (2014). Calculating melting temperatures and pressures of peridotite protoliths: Implications for the origin of cratonic mantle. *Earth and Planetary Science Letters*, *403*, 273–286.

Leeman, W. P., Smith, D. R., Hildreth, W., Palacz, Z., & Rogers, N. (1990). Compositional diversity of late Cenozoic basalts in a transect across the southern Washington cascades: Implications for subduction zone magmatism. *Journal of Geophysical Research*, *95*(B12), 19,561–19,582. https://doi.org/10.1029/JB095iB12p19561

Lu, Y., Makishima, A., & Nakamura, E. (2007). Coprecipitation of Ti, Mo, Sn and Sb with fluorides and application to determination of B, Ti, Zr, Nb, Mo, Sn, Sb, Hf and Ta by ICPMS. *Chemical Geology*, *236*(1), 13–26.

Macpherson, C. G., Dreher, S. T., & Thirlwall, M. F. (2006). Adakites without slab melting: High pressure differentiation of island arc magma, Mindanao, the Philippines. *Earth and Planetary Science Letters*, *243*(3-4), 581–593. https://doi.org/10.1016/j.epsl.2005.12.034

Mahony, S. H., Wallace, L. M., Miyoshi, M., Villamor, P., Sparks, R. S. J., & Hasenaka, T. (2011). Volcano-tectonic interactions during rapid plate-boundary evolution in the Kyushu region, SW Japan. *Geological Society of America Bulletin*, *123*(11–12), 2201–2223.

Makishima, A., & Nakamura, E. (2006). Determination of major/minor and trace elements in silicate samples by ICP-QMS and ICP-SFMS applying isotope dilution-internal standardization (ID-IS) and multi-stage internal standardisation. *Geostandards and Geoanalytical Research*, *30*(3), 245–271.
Makishima, A., Tanaka, R., & Nakamura, E. (2009). Precise elemental and isotopic analyses in silicate samples employing ICP-MS: Application of hydrofluoric acid solution and analytical techniques. *Analytical Sciences*, *25*(10), 1181–1187.
Marín-Cerón, M. I., Moriguti, T., Makishima, A., & Nakamura, E. (2010). Slab decarbonation and CO_2 recycling in the southwestern Colombian volcanic arc. *Geochimica et Cosmochimica Acta*, *74*(3), 1104–1121.
Marsh, B. D. (1979). Island arc development: Some observations, experiments, and speculations. *The Journal of Geology*, *87*(6), 687–713.
Martin, H. (1999). Adakitic magmas: Modern analogues of Archaean granitoids. *Lithos*, *46*(3), 411–429.
Martin, H., Smithies, R., Rapp, R., Moyen, J.-F., & Champion, D. (2005). An overview of adakite, tonalite-trondhjemite-granodiorite (TTG), and sanukitoid: Relationships and some implications for crustal evolution. *Lithos*, *79*(1-2), 1–24.
Mason, W. G., Moresi, L., Betts, P. G., & Miller, M. S. (2010). Three-dimensional numerical models of the influence of a buoyant oceanic plateau on subduction zones. *Tectonophysics*, *483*(1), 71–79.
Matsui, S., & Inoue, T. (1970). ^{14}C age of ejecta of Sanbe volcano-^{14}C age of the Quaternary deposits in Japan (56). *Earth Science (Chikyu Kagaku)*, *24*, 112–114.
Matsumoto, A., Itoh, J., Hishizumi, H., & Ohta, Y. (2010). K-Ar and $^{40}Ar/^{39}Ar$ ages of Himeshima Volcanic Group, Kyushu, Japan. In *Programme and abstracts the Volcanological Society of Japan* (40 pp.). Tokyo: Volcanological Society of Japan.
Matsuura, H. (1986). K-Ar age of an alkali basalt from Mt. Mengame, Hiroshima prefecture. *Journal of the Geological Society of Japan*, *92*(3), 235–237. https://doi.org/10.5575/geosoc.92.235
Matsuura, H., & Tsuchiya, N. (2003). Early Pleistocene Moritayama lava: An Old-Sambe Volcano. *Volcano (Kazan)*, *48*(1), 69–73.
McDonough, W. F., & Rudnick, R. L. (1998). Mineralogy and composition of the upper mantle. *Reviews in Mineralogy and Geochemistry*, *37*(1), 139.
McDonough, W. F., & Sun, S.-S. (1995). The composition of the Earth. *Chemical Geology*, *120*(3–4), 223–253. https://doi.org/10.1016/0009-2541(94)00140-4
McKenzie, D. (1984). The generation and compaction of partially molten rock. *Journal of Petrology*, *25*(3), 713–765.
McKenzie, D. (1985). The extraction of magma from the crust and mantle. *Earth and Planetary Science Letters*, *74*(1), 81–91.
Miura, C., & Sawai, O. (2010). K-Ar ages and geochemical characteristics of the Oe-Takayama volcanic products around the Iwami silver mine, Shimane prefecture, Japan. In *Annual Meeting of Japan Association of Mineralogical Sciences* (pp. 246–246). Sendai: Japan Association of Mineralogical Sciences.
Miyashiro, A. (1974). Volcanic rock series in island arcs and active continental margins. *American Journal of Science*, *274*(4), 321–355. https://doi.org/10.2475/ajs.274.4.321
Moriguti, T., Shibata, T., & Nakamura, E. (2004). Lithium, boron and lead isotope and trace element systematics of quaternary basaltic volcanic rocks in northeastern Japan: Mineralogical controls on slab-derived fluid composition. *Chemical Geology*, *212*(1-2), 81–100. https://doi.org/10.1016/j.chemgeo.2004.08.005
Moriyama, T. (2006), Geochemical and isotopic study of lower crustal xenoliths from Oki-Dogo, southwest Japan: Implications for the origin and evolution of the continental lower crust (PhD thesis). Okayama University, Misasa, Tottori, Japan.
Morris, P. A. (1995). Slab melting as an explanation of Quaternary volcanism and aseismicity in southwest Japan. *Geology*, *23*(5), 395–398. https://doi.org/10.1130/0091-7613(1995)023%3C0395:SMAAEO%3E2.3.CO;2
Morris, P. A., & Itaya, T. (1997). The Matsue formation: Evidence for gross mantle heterogeneity beneath southwest Japan at 11 Ma. *Island Arc*, *6*(4), 337–352. https://doi.org/10.1111/j.1440-1738.1997.tb00044.x
Morris, P. A., Itaya, T., Watanabe, T., & Yamauchi, S. (1990). Potassium/argon ages of Cenozoic igneous rocks from eastern Shimane prefecture Oki dozen island, southwest Japan and the Japan Sea opening. *Journal of Southeast Asian Earth Sciences*, *4*(2), 125–131.
Müntener, O., & Ulmer, P. (2006). Experimentally derived high-pressure cumulates from hydrous arc magmas and consequences for the seismic velocity structure of lower arc crust. *Geophysical Research Letters*, *33*, L21308. https://doi.org/10.1029/2006GL027629
Murayama, M. (1973). Geology of the Yokota district (Tech. Rep.). Geological Survey of Japan.
Murayama, M., & Ozawa, A. (1961). Geology of the Aoya and Kurayoshi districts (Tech. Rep.). Geological Survey of Japan.
Nagao, K., Ogata, A., Miura, Y. N., & Yamaguchi, K. (1996). Ar isotope analysis for K-Ar dating using two modified-VG5400 mass spectrometers—I: Isotope dilution method. *Journal of the Mass Spectrometry Society of Japan*, *44*(1), 39–61. https://doi.org/10.5702/massspec.44.39
Nagao, T., & Nishikawa, J.-I. (1980). $^{87}Sr/^{86}Sr$ ratios and their source materials of the volcanic rocks from the Pliocene Misasa Group in San-in District. *The Journal of the Japanese Association of Mineralogists, Petrologists and Economic Geologists*, *75*(10), 323–328.
Nakajima, J., & Hasegawa, A. (2007). Tomographic evidence for the mantle upwelling beneath southwestern Japan and its implications for arc magmatism. *Earth and Planetary Science Letters*, *254*(1), 90–105.
Nakamura, E., Campbell, I. H., McCulloch, M. T., & Sun, S.-S. (1989). Chemical geodynamics in a back arc region around the Sea of Japan: Implications for the genesis of alkaline basalts in Japan, Korea, and China. *Journal of Geophysical Research*, *94*(B4), 4634–4654. https://doi.org/10.1029/JB094iB04p04634
Nakamura, E., Campbell, I. H., & Sun, S.-S. (1985). The influence of subduction processes on the geochemistry of Japanese alkaline basalts. *Nature*, *316*(6023), 55–58. https://doi.org/10.1038/316055a0
Nakamura, E., Makishima, A., Moriguti, T., Kobayashi, K., Sakaguchi, C., Yokoyama, T., et al. (2003). Comprehensive geochemical analyses of small amounts (~100 mg) of extraterrestrial samples for the analytical competition related to the sample return mission MUSES-C, The Institute of Space and Astronautical Science Report. SP No. 16, 49–101.
Nakamura, E., McCulloch, M. T., & Campbell, I. H. (1990). Chemical geodynamics in the back-arc region of Japan based on the trace element and Sr-Nd isotopic compositions. *Tectonophysics*, *174*(3–4), 207–233. https://doi.org/10.1016/0040-1951(90)90323-Z
Nakamura, E., McDougall, I., & Campbell, I. H. (1986). K-Ar ages of basalts from the Higashi-Matsuura district, northwestern Kyushu, Japan and regional geochronology of the Cenozoic alkaline volcanic rocks in eastern Asia. *Geochemical Journal*, *20*(2), 91–99. https://doi.org/10.2343/geochemj.20.91
Nier, A. O. (1950). A redetermination of the relative abundances of the isotopes of carbon, nitrogen, oxygen, argon, and potassium. *Physical Review*, *77*(6), 789–793. https://doi.org/10.1103/PhysRev.77.789
Nishiki, K., Itoh, J.-I., & Ueno, T. (2012). Database of Quaternary volcanic and intrusive rock bodies in Japan [CD-ROM], 60, Geological Survey of Japan Interim Report, Geological Survey of Japan, AIST, Japan.
Nozaka, T. (1997). Structure and development of the lower crust and upper mantle of southwestern Japan: Evidence from petrology of deep-seated xenoliths. *Island Arc*, *6*(4), 404–420. https://doi.org/10.1111/j.1440-1738.1997.tb00050.x

Ohba, T., Matsuoka, K., Kimura, Y., Ishikawa, H., & Fujimaki, H. (2009). Deep crystallization differentiation of arc tholeiite basalt magmas from northern Honshu arc, Japan. *Journal of Petrology*, *50*(6), 1025–1046.

Okino, K., Shimakawa, Y., & Nagaoka, S. (1994). Evolution of the Shikoku Basin. *Journal of Geomagnetism and Geoelectricity*, *46*(6), 463–479.

Peacock, S. M. (2009). Thermal and metamorphic environment of subduction zone episodic tremor and slip. *Journal of Geophysical Research*, *114*, B00A07. https://doi.org/10.1029/2008JB005978

Peacock, S. M., & Wang, K. (1999). Seismic consequences of warm versus cool subduction metamorphism: Examples from southwest and northeast Japan. *Science*, *286*(5441), 937–939. https://doi.org/10.1126/science.286.5441.937

Perfit, M. R., Gust, D. A., Bence, A. E., Arculus, R. J., & Taylor, S. R. (1980). Chemical characteristics of island-arc basalts: Implications for mantle sources. *Chemical Geology*, *30*(3), 227–256.

Pertermann, M., & Hirschmann, M. M. (2003). Anhydrous partial melting experiments on MORB-like eclogite: Phase relations, phase compositions and mineral-melt partitioning of major elements at 2–3 GPa. *Journal of Petrology*, *44*(12), 2173–2201.

Pineda-Velasco, I., Nguyen, T. T., Kitagawa, H., & Nakamura, E. (2015). Comment on "Diverse magmatic effects of subducting a hot slab in SW Japan: Results from forward modeling?" by J.-I. Kimura et al. *Geochemistry, Geophysics, Geosystems*, *16*, 2848–2852. https://doi.org/10.1002/2015GC005914

Plank, T., & Langmuir, C. H. (1998). The chemical composition of subducting sediment and its consequences for the crust and mantle. *Chemical Geology*, *145*(3), 325–394.

Poli, S., & Schmidt, M. W. (2002). Petrology of subducted slabs. *Annual Review of Earth and Planetary Sciences*, *30*(1), 207–235.

Portnyagin, M., Hoernle, K., Plechov, P., Mironov, N., & Khubunaya, S. (2007). Constrains on mantle melting and composition and nature of slab components in volcanic arcs from volatiles (H_2O, S, Cl, F) and trace elements in melt inclusions from the Kamchatka Arc. *Earth and Planetary Science Letters*, *255*(1–2), 53–69.

Qian, Q., & Hermann, J. (2013). Partial melting of lower crust at 10–15 kbar: Constraints on adakite and TTG formation. *Contributions to Mineralogy and Petrology*, *165*(6), 1195–1224. https://doi.org/10.1007/s00410-013-0854-9

Rapp, R. P. (1995). Amphibole-out phase boundary in partially melted metabasalt, its control over liquid fraction and composition, and source permeability. *Journal of Geophysical Research*, *100*(B8), 15,601–15,610. https://doi.org/10.1029/95JB00913

Rapp, R. P., & Watson, E. B. (1995). Dehydration melting of metabasalt at 8–32 kbar: Implications for continental growth and crust-mantle recycling. *Journal of Petrology*, *36*(4), 891–931. https://doi.org/10.1093/petrology/36.4.891

Rapp, R. P., Watson, E. B., & Miller, C. F. (1991). Partial melting of amphibolite/eclogite and the origin of Archean trondhjemites and tonalites. *Precambrian Research*, *51*(1), 1-4–1-25.

Ribeiro, J. M., Maury, R. C., & Grégoire, M. (2016). Are adakites slab melts or high-pressure fractionated mantle melts? *Journal of Petrology*, *57*(5), 839–862. https://doi.org/10.1093/petrology/egw023

Ringwood, A. E. (2013). Petrogenesis in island arc systems. In M. Talwani, & W. C. Pitman (Eds.), *Island arcs, deep sea trenches and back-arc basins* (pp. 311–324). https://doi.org/10.1029/ME001p0311

Robinson, J. A. C., Wood, B. J., & Blundy, J. D. (1998). The beginning of melting of fertile and depleted peridotite at 1.5 GPa. *Earth and Planetary Science Letters*, *155*(1–2), 97–111.

Ryan, J. G., Leeman, W. P., Morris, J. D., & Langmuir, C. H. (1996). The boron systematics of intraplate lavas: Implications for crust and mantle evolution. *Geochimica et Cosmochimica Acta*, *60*(3), 415–422.

Sajona, F. G., Maury, R. C., Bellon, H., Cotten, J., & Defant, M. (1996). High field strength element enrichment of Pliocene-Pleistocene Island arc basalts, Zamboanga peninsula, western Mindanao (Philippines). *Journal of Petrology*, *37*(3), 693–726.

Sakoda, M., Kodama, T., & Inoue, T. (2000). Mineralization and K-Ar ages of the Ohmori (Iwami) Au-Cu-Ag vein-type deposits, Shimane prefecture, southwest Japan. *Resource Geology*, *50*, 45–60.

Sakuyama, M., & Nesbitt, R. (1986). Geochemistry of the Quaternary volcanic rocks of the Northeast Japan arc. *Journal of Volcanology and Geothermal Research*, *29*(1), 413–450.

Sakuyama, T., Nakai, S., Yoshikawa, M., Shibata, T., & Ozawa, K. (2014). Progressive interaction between dry and wet mantle during high-temperature diapiric upwelling: Constraints from Cenozoic Kita-Matsuura Intraplate Basalt Province, northwestern Kyushu, Japan. *Journal of Petrology*, *55*(6), 1083–1128.

Sato, D., Matsumoto, I., & Kamei, A. (2011). Petrography and bulk rock composition of the Wakurayama Dacite from Matsue City, Shimane prefecture, southwest Japan. *Journal of the Geolollical Society of Japan*, *117*(8), 439–450.

Sen, C., & Dunn, T. (1994). Dehydration melting of a basaltic composition amphibolite at 1.5 and 2.0 GPa: Implications for the origin of adakites. *Contributions to Mineralogy and Petrology*, *117*(4), 394–409.

Shaw, D. M. (1970). Trace element fractionation during anatexis. *Geochimica et Cosmochimica Acta*, *34*(2), 237–243.

Shibata, T., & Nakamura, E. (1997). Across-arc variations of isotope and trace element compositions from Quaternary basaltic volcanic rocks in northeastern Japan: Implications for interaction between subducted oceanic slab and mantle wedge. *Journal of Geophysical Research*, *102*(B4), 8051–8064. https://doi.org/10.1029/96JB03661

Shibata, T., Yoshikawa, M., Itoh, J.-I., Ujike, O., Miyoshi, M., & Takemura, K. (2014). Along-arc geochemical variations in Quaternary magmas of northern Kyushu Island, Japan. In A. Gómez-Tuena, S. M. Straub, & G. F. Zellmer (Eds.), *Orogenic andesites and crustal growth*. *Geological Society of London, Special Publications, 385*, 15–29.

Shimoda, G., Tatsumi, Y., & Morishita, Y. (2003). Behavior of subducting sediments beneath an arc under a high geothermal gradient: Constraints from the Miocene SW Japan arc. *Geochemical Journal*, *37*(4), 503–518.

Shimoda, G., Tatsumi, Y., Nohda, S., Ishizaka, K., & Jahn, B. (1998). Setouchi high-Mg andesites revisited: Geochemical evidence for melting of subducting sediments. *Earth and Planetary Science Letters*, *160*(3), 479–492.

Shukuno, H., & Arai, S. (1999). Olivine-chromian spinel compositional relationships of the Cenozoic alkali basalts from southwest Japan: Implication for their mantle restites. *Journal of Mineralogy Petrology and Economic Geology*, *94*(4), 120–140. https://doi.org/10.2465/ganko.94.120

Springer, W., & Seck, H. A. (1997). Partial fusion of basic granulites at 5 to 15 kbar: Implications for the origin of TTG magmas. *Contributions to Mineralogy and Petrology*, *127*(1–2), 30–45. https://doi.org/10.1007/s004100050263

Steiger, R., & Jäger, E. (1977). Subcommission on geochronology: Convention on the use of decay constants in geo- and cosmochronology. *Earth and Planetary Science Letters*, *36*(3), 359–362.

Stevenson, D. J. (1994). Weakening under stress. *Nature*, *372*(6502), 129–130. https://doi.org/10.1038/372129a0

Stolper, E., Walker, D., Hager, B. H., & Hays, J. F. (1981). Melt segregation from partially molten source regions: The importance of melt density and source region size. *Journal of Geophysical Research*, *86*(B7), 6261–6271. https://doi.org/10.1029/JB086iB07p06261

Straub, S. M., Goldstein, S. L., Class, C., Schmidt, A., & Gomez-Tuena, A. (2010). Slab and mantle controls on the Sr-Nd-Pb-Hf isotope evolution of the post 42 Ma Izu-Bonin volcanic arc. *Journal of Petrology*, *51*(5), 993–1026.

Sugimoto, T., Shibata, T., Yoshikawa, M., & Takemura, K. (2006). Sr-Nd-Pb isotopic and major and trace element compositions of the Yufu-Tsurumi volcanic rocks: Implications for the magma genesis of the Yufu-Tsurumi volcanoes, northeast Kyushu, Japan. *Journal of Mineralogical and Petrological Sciences*, *101*(5), 270–275.

Syracuse, E. M., van Keken, P. E., & Abers, G. A. (2010). The global range of subduction zone thermal models. *Physics of the Earth and Planetary Interiors*, *183*(1), 73–90.

Takahashi, E. (1978). Petrologic model of the crust and upper mantle of the Japanese island arcs. *Bulletin Volcanologique*, *41*(4), 529–547.

Takahashi, T., Hirahara, Y., Miyazaki, T., Senda, R., Chang, Q., Kimura, J.-I., & Tatsumi, Y. (2013). Primary magmas at the volcanic front of the NE Japan arc: Coeval eruption of crustal low-k tholeiitic and mantle-derived medium-k calc-alkaline basalts at Azuma volcano. *Journal of Petrology*, *54*(1), 103–148.

Takei, H. (2002). Development of precise analytical techniques for major and trace element concentrations in rock samples and their applications to the Hishikari gold mine, southern Kyushu, Japan (PhD thesis). Okayama University, Okayama.

Tamura, Y., Yuhara, M., & Ishii, T. (2000). Primary arc basalts from Daisen volcano, Japan: Equilibrium crystal fractionation versus disequilibrium fractionation during supercooling. *Journal of Petrology*, *41*(3), 431–448.

Tamura, Y., Yuhara, M., Ishii, T., Irino, N., & Shukuno, H. (2003). Andesites and dacites from Daisen volcano, Japan: Partial-to-total remelting of an andesite magma body. *Journal of Petrology*, *44*(12), 2243–2260.

Tanaka, T., Togashi, S., Kamioka, H., Amakawa, H., Kagami, H., Hamamoto, T., et al. (2000). JNdi-1: A neodymium isotopic reference in consistency with La Jolla neodymium. *Chemical Geology*, *168*(3), 279–281.

Tatsumi, Y., Arai, R., & Ishizaka, K. (1999). The petrology of a melilite-olivine nephelinite from Hamada, SW Japan. *Journal of Petrology*, *40*(4), 497–509.

Tatsumi, Y., & Koyaguchi, T. (1989). An absarokite from a phlogopite lherzolite source. *Contributions to Mineralogy and Petrology*, *102*(1), 34–40.

Tatsumi, Y., Takahashi, T., Hirahara, Y., Chang, Q., Miyazaki, T., Kimura, J.-I., et al. (2008). New insights into andesite genesis: The role of mantle-derived calc-alkalic and crust-derived tholeiitic melts in magma differentiation beneath Zao volcano, NE Japan. *Journal of Petrology*, *49*(11), 1971–2008. https://doi.org/10.1093/petrology/egn055

Terakado, Y., Shimizu, H., & Masuda, A. (1988). Nd and Sr isotopic variations in acidic rocks formed under a peculiar tectonic environment in Miocene southwest Japan. *Contributions to Mineralogy and Petrology*, *99*(1), 1–10.

Toya, N., Ban, M., & Shinjo, R. (2005). Petrology of Aoso volcano, Northeast Japan arc: Temporal variation of the magma feeding system and nature of low-K amphibole andesite in the Aoso-Osore volcanic zone. *Contributions to Mineralogy and Petrology*, *148*(5), 566–581.

Tsuchiyama, A. (1985). Dissolution kinetics of plagioclase in the melt of the system diopside albite-anorthite, and origin of dusty plagioclase in andesites. *Contributions to Mineralogy and Petrology*, *89*(1), 1–16.

Tsukui, M. (1984). Geology of Daisen volcano. *Journal of the Geological Society of Japan*, *90*, 643–658.

Tsukui, M. (1985). Temporal variation in chemical composition of phenocrysts and magmatic temperature at Daisen volcano, southwest Japan. *Journal of Volcanology and Geothermal Research*, *26*(3–4), 317–336.

Tsukui, M., Nishido, H., & Nagao, K. (1985). K-Ar ages of the Hiruzen volcano group and the Daisen volcano. *Journal of the Geological Society of Japan*, *91*(4), 279–288. https://doi.org/10.5575/geosoc.91.279

Ueki, K., & Iwamori, H. (2017). Geochemical differentiation processes for arc magma of the Sengan volcanic cluster, northeastern Japan, constrained from principal component analysis. *Lithos*, *290*, 60–75.

Uto, K. (1990), Neogene volcanism of southwest Japan: Its time and space based on K-Ar dating (PhD thesis). University of Tokyo.

Uto, K., & Koyaguchi, T. (1987). K-Ar ages of three alkaline basalts from the Abu Monogenetic Volcano Group, southwest Japan. *Bulletin of the Volcanological Society of Japan, Second Series*, *32*(3), 263–267.

Walker, D., Shibata, T., & DeLong, S. E. (1979). Abyssal tholeiites from the oceanographer fracture zone. *Contributions to Mineralogy and Petrology*, *70*(2), 111–125.

Walowski, K. J., Wallace, P. J., Hauri, E. H., Wada, I., & Clynne, M. A. (2015). Slab melting beneath the Cascade Arc driven by dehydration of altered oceanic peridotite. *Nature Geoscience*, *8*(5), 404–408.

Weis, D., Kieffer, B., Maerschalk, C., Barling, J., de Jong, J., Williams, G. A., et al. (2006). High-precision isotopic characterization of USGS reference materials by TIMS and MC-ICP-MS. *Geochemistry, Geophysics, Geosystems*, *7*, Q08006. https://doi.org/10.1029/2006GC001283

Wessel, P., Smith, W. H., Scharroo, R., Luis, J., & Wobbe, F. (2013). Generic Mapping Tools: Improved version released. *Eos, Transactions American Geophysical Union*, *94*(45), 409–410. https://doi.org/10.1002/2013EO450001

Workman, R. K., & Hart, S. R. (2005). Major and trace element composition of the depleted MORB mantle (DMM). *Earth and Planetary Science Letters*, *231*(1-2), 53–72. https://doi.org/10.1016/j.epsl.2004.12.005

Xu, J.-F., Shinjo, R., Defant, M. J., Wang, Q., & Rapp, R. P. (2002). Origin of Mesozoic adakitic intrusive rocks in the Ningzhen area of East China: Partial melting of delaminated lower continental crust? *Geology*, *30*(12), 1111–1114.

Yamamoto, M. (1988). Picritic primary magma and its source mantle for Oshima-Ōshima and back-arc side volcanoes, northeast Japan arc. *Contributions to Mineralogy and Petrology*, *99*(3), 352–359.

Yamamoto, T. (2017). Quantitative eruption history of Pleistocene Daisen volcano, SW Japan. *Bulletin of the Geological Survey of Japan*, *68*(1), 1–16.

Yamane, N., Kanagawa, K., & Ito, T. (2012). Contrasting seismic reflectivity of the lower crust and uppermost mantle between NE Japan and SW Japan as illustrated by petrophysical analyses of mafic and ultramafic xenoliths. *Journal of Geophysical Research*, *117*, B09203. https://doi.org/10.1029/2011JB009008

Yasuda, A., Fujii, T., & Kurita, K. (1994). Melting phase relations of an anhydrous mid-ocean ridge basalt from 3 to 20 GPa: Implications for the behavior of subducted oceanic crust in the mantle. *Journal of Geophysical Research*, *99*(B5), 9401–9414.

Yaxley, G. M., & Green, D. H. (1998). Reactions between eclogite and peridotite: Mantle refertilisation by subduction of oceanic crust. *Schweizerische Mineralogische und Petrographische Mitteilungen*, *78*(2), 243–255.

Yogodzinski, G. M., Brown, S. T., Kelemen, P. B., Vervoort, J. D., Portnyagin, M., Sims, K. W. W., et al. (2015). The role of subducted basalt in the source of island arc magmas: Evidence from seafloor lavas of the western Aleutians. *Journal of Petrology*, *56*(3), 441–492.

Yogodzinski, G. M., Kay, R. W., Volynets, O. N., Koloskov, A. V., & Kay, S. M. (1995). Magnesian andesite in the western Aleutian Komandorsky region: Implications for slab melting and processes in the mantle wedge. *Geological Society of America Bulletin*, *107*(5), 505–519.

Yogodzinski, G. M., Kelemen, P. B., Hoernle, K., Brown, S. T., Bindeman, I., Vervoort, J. D., et al. (2017). Sr and O isotopes in western Aleutian seafloor lavas: Implications for the source of fluids and trace element character of arc volcanic rocks. *Earth and Planetary Science Letters*, *475*, 169–180.

Yogodzinski, G. M., Lees, J. M., Churikova, T. G., Dorendorf, F., Wöerner, G., & Volynets, O. N. (2001). Geochemical evidence for the melting of subducting oceanic lithosphere at plate edges. *Nature*, *409*(6819), 500–504.

Yokoyama, T., Kobayashi, K., Kuritani, T., & Nakamura, E. (2003). Mantle metasomatism and rapid ascent of slab components beneath island arcs: Evidence from ^{238}U-230Th-^{226}Ra disequilibria of Miyakejima volcano, Izu arc, Japan. *Journal of Geophysical Research*, *108*(B7), 2329. https://doi.org/10.1029/2002JB002103

Yokoyama, T., Makishima, A., & Nakamura, E. (1999). Evaluation of the coprecipitation of incompatible trace elements with fluoride during silicate rock dissolution by acid digestion. *Chemical Geology*, *157*(3), 175–187.

Yokoyama, T., & Nakamura, E. (2002). Precise determination of ferrous iron in silicate rocks. *Geochimica et Cosmochimica Acta*, *66*(6), 1085–1093. https://doi.org/10.1016/S0016-7037(01)00809-2

Yoshikawa, M., & Nakamura, E. (1993). Precise isotope determination of trace amounts of Sr in magnesium-rich samples. *Journal of Mineralogy Petrology and Economic Geology*, *88*(12), 548–561.

Zellmer, G. F., Hwang, S.-L., Sakamoto, N., Iizuka, Y., Harada, S., Kimura, J.-I., et al. (2015). Interaction of arc magmas with subvolcanic hydrothermal systems: Insights from compositions and metasomatic textures of olivine crystals in fresh basalts of Daisen and Mengameyama, western Honshu, Japan. In G. F. Zellmer, M. Edmonds, & S. M. Straub (Eds.), *The role of volatiles in the genesis, evolution and eruption of arc magmas*. *Geological Society of London, Special Publications, 410*, 219–236.

Zellmer, G. F., Iizuka, Y., Miyoshi, M., Tamura, Y., & Tatsumi, Y. (2012). Lower crustal H_2O controls on the formation of adakitic melts. *Geology*, *40*(6), 487–490.

Zellmer, G. F., Sakamoto, N., Iizuka, Y., Miyoshi, M., Tamura, Y., Hsieh, H.-H., & Yurimoto, H. (2014). Crystal uptake into aphyric arc melts: Insights from two-pyroxene pseudodecompression paths, plagioclase hygrometry, and measurement of hydrogen in olivines from mafic volcanics of SW Japan. In A. Gómez-Tuena, S. M. Straub, & G. F. Zellmer (Eds.), *Orogenic andesites and crustal growth*. *Geological Society of London, Special Publications, 385*, 161–184.

Zhao, D., Liu, X., & Hua, Y. (2018). Tottori earthquakes and Daisen volcano: Effects of fluids, slab melting and hot mantle upwelling. *Earth and Planetary Science Letters*, *485*, 121–129.

Zhao, D., Yanada, T., Hasegawa, A., Umino, N., & Wei, W. (2012). Imaging the subducting slabs and mantle upwelling under the Japan Islands. *Geophysical Journal International*, *190*(2), 816–828.